DYNAMIC CORTICAL ACTIN CONTRACTIONS DURING CONVERGENCE AND EXTENSION OF FROG EMBRYO

by

Hye Young Kim

Bachelor of Science, Sung Kyun Kwan University, 2003

Master of Science, Drexel University, 2006

Submitted to the Graduate Faculty of

Swanson School of Engineering in partial fulfillment

of the requirements for the degree of

Doctor of Philosophy

University of Pittsburgh

2011

UNIVERSITY OF PITTSBURGH

SWANSON SCHOOL OF ENGINEERING

This dissertation was presented

by

Hye Young Kim

It was defended on

November, 9, 2010

and approved by

Philip Leduc, Associate Professor, Department of Mechanical Engineering

Partha Roy, Associate Professor, Department of Bioengineering

James Wang, Associate Professor, Department of Mechanical Engineering and Materials Science

Dissertation Director: Lance Davidson, Assistant Professor, Department of Bioengineering

DYNAMIC CORTICAL ACTIN CONTRACTIONS DURING CONVERGENCE AND EXTENSION OF FROG EMBRYO

Hye Young Kim, PhD

University of Pittsburgh, 2011

Actomyosin networks linked to the micro-environment through the plasma membrane are thought to be key players regulating cell behaviors. Even after decades of studies dedicated to reveal the role of actin cytoskeleton in single cell migrations, we do not understand how actomyosin networks drive cell movements within multicellular tissues, like those in developing embryos. Here we use the converging and extending mesoderm tissues of Xenopus embryo as a model system to understand the role of cortical actin cytoskeleton during cell rearrangement within a multicellular organism.

Using high resolution live imaging of F-actin, we observe the unique dynamic actin contractions called "punctuated actin contractions" in the mid-cell body of mesenchymal cells. These contraction dynamics are a common feature of *Xenopus* embryonic cells and mediate cell shape changes during morphogenesis. Quantitative morphological analysis of these F-actin dynamics indicates that frequent and aligned movements of multiple actin contractions accompany mesoderm cells as they intercalate and elongate. Moreover, we found levels of punctuated actin contractions are permissively regulated by the non canonical Wnt-signaling pathway. Over-expression on Xfz7 can induce early maturation of actin contractions in mesoderm and produce mesoderm-like actin contractions in ectoderm cells. In contrast, expression of the dominant negative Disheveled constructs Xdd1 block the progression of actin contractions to their late mesoderm dynamics, it but has no effect in ectoderm. Additionally, using inhibitors combined with FRAP analysis we find the dynamics of actin contractions are

regulated by both myosin contractility and F-actin polymerization. We also show the actin contractions can be induced by microtubules via RhoGEFs in mesoderm tissue.

In summary, this study reveals punctuated actin contractions within converging and extending mesoderm, and uncovers permissive roles for non-canonical Wnt-signaling, myosin contractility, and F-actin polymerization which play a role in regulating those dynamics.

TABLE OF CONTENTS

LIST OF TABLES

LIST OF FIGURES

PREFACE

Often people recall the period of doctorate as a long and tough time of their life. However, I could enjoy myself and succeed to finish my dissertation with enormous supports of people around me. First I would like to heartily thank my mentor, Dr. Lance Davidson. I was fortunate to meet him as an advisor who always encourages and guide me to grow as a researcher. My dissertation committee advisors, Dr. Philip Leduc, Dr. James Wang, and Dr. Partha Roy, your constructive criticisms and comments help to strengthen my research projects and myself. I deeply thank you all.

I cannot imagine how I could come through without my lab mates, Sagar, Jian, Mickey, and Lin. You were my friends, family, and mentors in Pittsburgh.

I would like to thank my family, Bae Sung Kim, Myoung Ja Joo, and Hye Sun Kim. I love you. You are my power of life.

I just have a first step toward a new road that opens in many ways. I believe this dissertation work will provide the basis for my continuing exploration. I hope I can continue to enjoy the next step of my life as a passionate mind of researcher and with my love, Seung Jun.

1.0 INTRODUCTION

1.1 CONVERGENCE AND EXTENSION

Morphogenesis is driven by collective cell migration. Groups of cells move as a coherent mass which simultaneously maintaining cell-cell contacts as they generate active protrusions during morphogenesis, wound healing, and cancer metastasis. Although studies over the past 20 years have established modes of single cell migration (Lauffenburger and Horwitz 1996), we do not understand how groups of cells in tissues are motile yet simultaneously connected by cell-cell junctions.

One of the appealing model systems to study coordinated cell movements is morphogenesis. This physical process for shaping the organism is accompanied by controlled cell rearrangements in a large cohesive population. Many organisms, including vertebrate share a common cellular process to establish the basic body plan. These cellular processes include directed movement of distinct populations of cells which result in narrowing and lengthening of the tissue, also known as convergence and extension (Figure 1A). Pioneering studies in frog development characterized mediolaterally directed cell intercalation during convergent extension, a process that builds the body axis of the frog embryo (Keller, Davidson et al. 2000). At the start of gastrulation, mesodermal cells around the marginal zone begin to invaginate into the embryo as they intercalate between neighbors. One round of intercalation proceeds dramatic shape

changes in the mesoderm tissue as well as whole embryo. Cell intercalation and shape changes begin in the anterior mesoderm and progress medially, laterally, and posteriorly (Figure 1B and C) (Shih and Keller 1992a; Shih and Keller 1992b). Eventually three to four rounds of cell intercalation are integrated to drive dorsal tissue elongation. Moreover, cell intercalation is associated with mediolaterally biased protrusions onto neighboring cell surfaces or extracellular matrix, and is thought to exert traction on them (Shih and Keller 1992a; Shih and Keller 1992b).

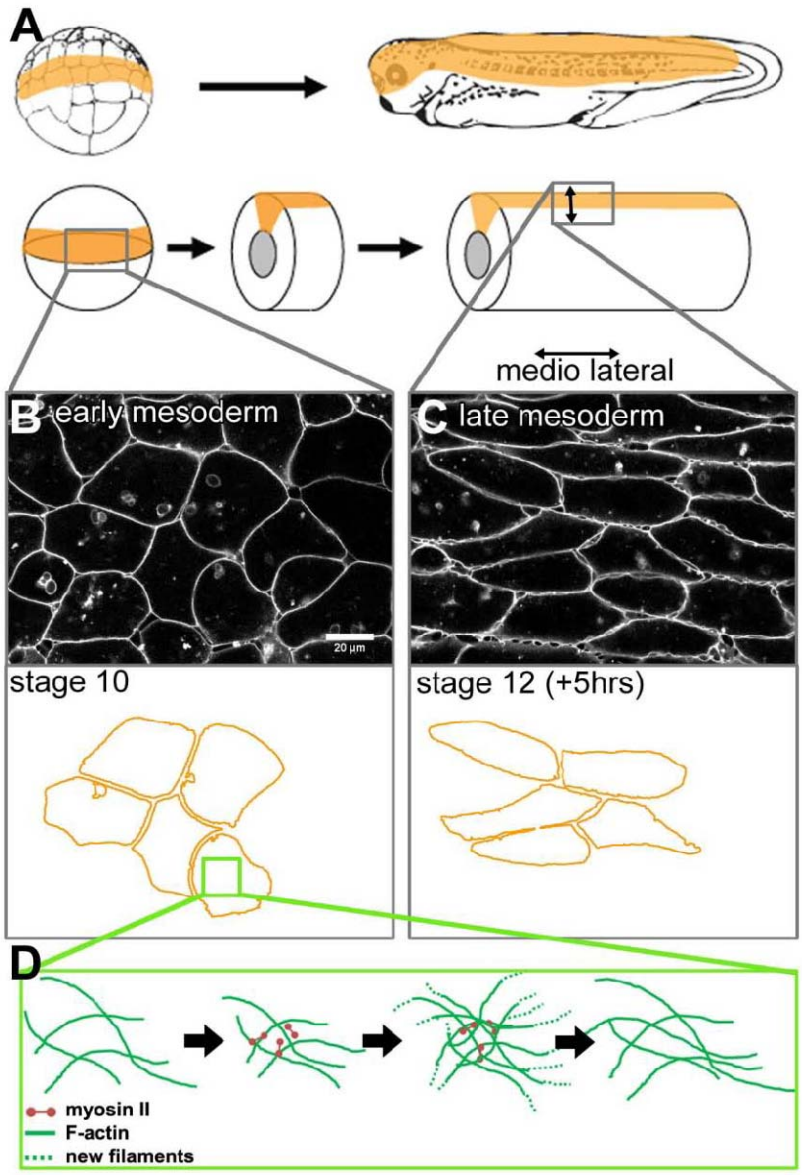

Figure 1. Convergence and extension

(A) A round Xenopus embryo develops into an elongated tadpole through convergent extension of the marginal zone area (shaded region) during gastrulation. (B-C) Mesoderm cells change shape from isometric to mediolaterally elongated ones. Cell boundaries were captured from mem-GFP expressing mesoderm tissue (B) at early gastrulation and (C) late gastrulation. (D) A proposed model for assembly of cortical actomyosin contractions within the mid-cell body.

1.2 DYNAMICS OF ACTIN CYTOSKELETON DURING CONVERGENCE AND EXTENSION

The actin cytoskeleton is essential in the mechanical processes driving morphogenesis and tissue remodeling. A dynamic actin cytoskeleton regulates cellular processes including cell protrusive activity, cell shape change, ECM assembly, and tissue stiffness (Lauffenburger and Horwitz 1996; Wozniak and Chen 2009; Zhou, Kim et al. 2009). F-actin polymerization at the leading edge of cells extend lamellipodial and filopodial protrusions. Such protrusions can operate as "sensors" of the cellular micro-environment that feed signals back to cells to exert tractive forces and direct cell migration (Geiger, Spatz et al. 2009). Rapid F-actin reorganization by polymerization, bundling, and branching is controlled by various actin binding proteins including myosin, and serve to maintain the mechanical integrity of the cell cortex, direct cell protrusions, and regulate many events within the cell such as cytokinesis (Effler, Iglesias et al. 2007; Reichl, Ren et al. 2008), apoptosis (Rosenblatt, Raff et al. 2001; Charras 2008; Slattum, McGee et al. 2009), and membrane trafficking (Liu, Kaksonen et al. 2006; Lanzetti 2007).

Although previous reports suggest that the F-actin cortex within pericellular regions of the cell may be as important to processes in cells and tissues as F-actin involved in active cellular protrusions, little attention has been on the dynamics of cortical F-actin during morphogenesis. Only recently the importance of dynamic actomyosin networks has been revealed in numerous morphogenetic movements including polarity establishment in fertilized egg of *C. elegans* (Cowan and Hyman 2007; Anderson, Gill et al. 2008), apical constriction in epithelial sheets and the ventral furrow formation of *Drosophila* (Martin, Kaschube et al. 2009), and convergence and extension of mesenchymal tissues in *Xenopus laevis* (Skoglund, Rolo et al. 2008). In addition, studies from *Drosophila* epithelial morphogenesis illustrate that the principle functions of

actomyosin in cells and multicellular tissues are to physically connect cells with their environment and to drive coordinated cell movements (Martin, Kaschube et al. 2009). Even with these advancements, the role of dynamics F-actin cortex, and how actomyosin accomplishes functions such as shaping mesenchymal tissues during convergent extension are still unknown.

1.3 REGULATION OF ACTIN DYNAMICS DURING CONVERGNECE AND EXTENSION

1.3.1 Non-canonical Wnt-signaling pathway

Non-canonical Wnt-signaling pathway which is also known as Planar cell polarity (PCP) pathway provides spatial information that is transmitted locally from one cell to next (Amonlirdviman, Khare et al. 2005). PCP is a conserved mechanism for establishing planar polarity in tissues and operates in various systems such as alignment of hairs and bristles in *Drosophilla* (Fanto and McNeill 2004), mediolateral rearrangements of mesoderm cells (Wallingford, Rowning et al. 2000), and directing neural crest migration in *Xenopus* (Carmona-Fontaine, Matthews et al. 2008). It has been proposed that a signal from one cell orients adjacent cells in response to polarity signaling cascade through Frizzeled (Fz) transmembrane receptor (Fanto and McNeill 2004; Zallen 2007). A number of molecules triggered by PCP pathway regulate mediolateral intercalation through cytoskeletal effectors (Liu, Sato et al. 2008), assembly of extracellular matrix (Goto, Davidson et al. 2005), and persisting cell adhesions (Witzel, Zimyanin et al. 2006).

Actin cytoskeleton is an important downstream target of non-canonical Wnt-pathway in *Xenopus* mesoderm cells (Sato, Khadka et al. 2006). The signal generated from Wnt, Fz and dishevelled (Dvl) activate RhoA and Rac1 in *Xenopus* embryo as well as in cultured cells, and is required for convergence and extension (Habas, Kato et al. 2001; Tahinci and Symes 2003) (Figure 2). In cultured cells, these small GTPases are well characterized in regulating the actin cytoskeleton during cell shape change and migration, and directs both forward protrusions and rearward contractions (Hall 2005). Research has begun to fill the gaps between the signaling and regulation of the actin cytoskeleton *in vivo.* For instance, the formin protein Damm1 binds to Disheveled (Dvl) leading to activation of RhoA, and driving cytoskeleton reorganization through profilin during the convergence and extension of *Xenopus* embryo (Khadka, Liu et al. ; Habas, Kato et al. 2001; Sato, Khadka et al. 2006). However, we do not understand details of molecular mechanism that underlie the dynamic cortical actin cytoekeleton during mesoderm tissue convergence and extension.

1.3.2 RhoGEF: reorganize actin cytoskeleton

GTPase effector (Guanine nucleotide–exchange factors (GEFs) ;(Miyakoshi, Ueno et al. 2004; Kwan and Kirschner 2005; Tanegashima, Zhao et al. 2008)) and GTPase activator protein (GAPs ; (Hyodo-Miura, Yamamoto et al. 2006)) are two factors that links the PCP pathway to the cytoskeleton. Small GTPases, such as RhoGTPases. act as molecular switches that exist in GDP bound inactive form, or GTP bound active form. The transition from GDP to GTP bound form interacts with effector proteins to trigger multiple cellular responses including actin cytoskeleton reorganization which induces changes in cell behaviors. More than 70 genes in human encodes GEF family members (Rossman, Der et al. 2005), several GEFs including xNET1(RhoA specific

GEF; (Miyakoshi, Ueno et al. 2004)), Weak similarity GEF (WGEF;(Tanegashima, Zhao et al. 2008)), and XLfc (microtubule binding Rho GEF;(Kwan and Kirschner 2005) appear to mediate Rho activation during the convergence and extension of *Xenopus*. Although these GEFs are shown to lead to defects in axis elongation and link to components in non-canonical Wnt-signals, there has been no direct evidence that GEF activation is involved in remodeling actin cytoskeleton, or whatever its function is that is critical for cellular process during tissue convergence and extension.

1.3.3 Myosin: crosslink and contract the actin cytoskeleton

The assembly and disassembly of actin filaments and their organization into functional higher order networks are regulated by many actin-binding proteins (ABPs). For instance, new actin filaments can be nucleated with Arp2/3 complex, and filaments length is regulated by the capping protein, gelsolin that blocks addition of new monomers (Pollard and Cooper 1986; Pollard 2007). Filamentous actin organizes into a network through the activation of bundling and crosslinking ABPs like fimbrin, alpha-actinin, and filamin. The organized actin network provides physical support to the cell by anchoring filaments to the cell's membrane. This physical support connects to other cytoskeletal proteins, and produces contraction of linked filaments through cross linking proteins like myosin II.

Among actin binding proteins, the motor protein myosin is particularly important for cell polarization. As a cell migrates, it establishes a distinct front with protrusive lamellipodia and filopodia array, as well as the contractile rear that is organized by myosin II. Both front and rear regions are actin rich structures (Laevsky and Knecht 2003). The thin layer of the contractile cortex underneath of plasma membrane is called the contractile cortex (Bray and White 1988),

recognized in asymmetric deformation of cytoplasm *in vitro* (Paluch, van der Gucht et al. 2006), during cytokinesis (Zhou and Wang 2008), and cell division in *C.elegance* (Anderson, Gill et al. 2008). Furthermore, reorganization of the actin myosin network is required in morphogenetic movements such as *Drosophila* gastrulation (Martin, Kaschube et al. 2009) and convergence and extension in *Xenopus* (Skoglund, Rolo et al. 2008). Even though these detailed molecular dynamics of actin myosin networks and its function in controlling polarized cell shape suggest the importance of myosin contractility in mediolateral intercalation of mesoderm cells within the embryo, we have limited understanding on how the dynamics of myosin mediated contractile cortex are organized or regulated to control cell shape changes during these movements (Figure 2).

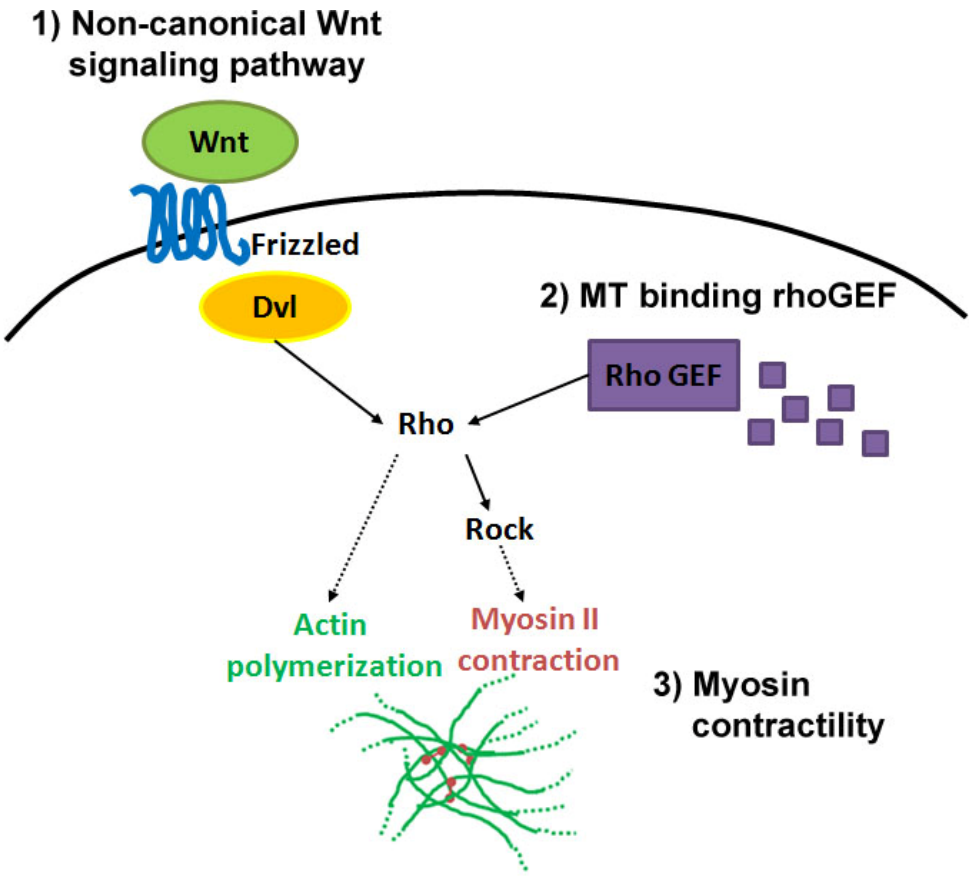

Figure 2. Regulation of actin dynamics during convergence and extension

Three possible regulation pathways exists which can control the dynamics of cortical F-actin contractions during convergence and extension of *Xenopus* embryo.

1.4 SIGNIFICANCE

Normal development of vertebrate embryos requires orchestrated changes in cell fate and movement. Cell fate is controlled by cellular signaling pathways through relevant gene expressions at desired stages and regions. Cell movement is powered by the cytoskeleton. To gain better understanding of developmental processes, we need a comprehensive insight of the integrated processes that control gene expression and cellular behaviors. One example of a developmental process that integrates gene and cell behaviors is neural tube closure which requires successful tissue convergence and extension. Failure of neural tube closure is responsible for neural tube defects (NTDs). NTDs are the most common human birth defects occurring in 1 out of every 1000 births (Copp, Greene et al. 2003). Studies have focused on the genetic causes of NTDs and have uncovered many critical genes and signaling pathways that regulate neural induction, patterning, and shaping of tissues (De Marco, Merello et al. 2006; Wallingford 2006). However, a clear understanding of the cellular mechanisms that lead to malformed tissues is lacking. Our efforts to investigate cellular mechanisms and the physical molecular machinery that regulates mediolateral cell intercalation, the basis of cellular behavior which drives neural tube closure, will improve current knowledge by complementing genomics data.

There are several advantages to using the developing frog embryo as a model system. Frog embryos and microsurgically prepared explants allow us to manipulate tissue architecture and cellular behaviors after applying pharmacological reagents, expressing novel proteins, and injecting morpholinos. Robust and rapid development occurs identically after fertilization in a large clutch of eggs from the same mated parents. Furthermore, cell movement and tissue remodel within the entire 3-D tissue illustrate the dynamic interaction of cells with the

extracellular matrix that tissue engineers aim to emulate when constructing new tissues for tissue regeneration *in vivo*.

1.5 SPECIFIC AIMS OF THE STUDY

The goal of this dissertation is to understand the dynamics of actin cytoskeleton that underlie the mediolateral cell intercalation behaviors during convergence and extension of frog embryo. Mediolateral cell intercalation is a form of cell motility that mesodermal cells use to rearrange themselves by extending active protrusions in medial and lateral directions, and then intercalate between neighbors. Moreover, the ability of cell behaviors to shape the embryo requires the dynamic actin cytoskeleton that connects the inside of the cell to its surroundings through cell-substrate and cell-cell adhesions.

To understand the role of dynamic actin cytoskeleton during tissue convergence and extension, we aim to investigate the nature of the cortical F-actin dynamics within mesoderm tissue, reveal its role during cell intercalation, and understand the mechanisms that regulate these dynamics.

These three specific aims are entitled below and are addressed in chapters 3, 4, and 5.

Aim I: Investigate the dynamics of actin cytoskeleton that mediate mediolateral cell intercalation behaviors

To begin to understand the role of the dynamic actin cytoskeleton in embryonic tissue, we will first examine what are the dynamics of cortical F-actin within embryo and microsursically isolated tissues. Using confocal time-lapse imaging combined with custom image analysis tools we quantify the dynamics of F-actin, and identify the intrinsic biophysical properties of F-actin within embryonic cells. In addition, we will test the relationship between the cortical F-actin dynamics and cell behaviors, and characterize the dynamics within different cell types and at different stages during convergence and extension.

Aim II: Investigate the role of non-canonical Wnt signaling pathway in regulating the dynamics of cortical F-actin contractions during convergence and extension

The non-canonical Wnt signaling pathway is thought to control the polarity of mesoderm and neural ectoderm tissue when cells elongate in the mediolateral direction during convergence and extension, and to send signals to actin cytoskeleton. We will investigate how the cortical actin contractions are regulated by the non-canonical Wnt-signals by inhibiting and activating this signaling pathway.

Aim III: Investigate the molecular control of dynamics of cortical F-actin contractions

Using either small molecule inhibitors or over expression of signaling proteins we will examine contributions of F-actin polymerization and myosin activity to assemble the dynamic F-actin contractions during convergence and extension. Live confocal imaging accompanied with fluorescent recovery after photo bleach (FRAP) will enable us to inspect the molecular dynamics of F-actin. Furthermore, we will examine the cell tractions generated by actin contractions using a force reporting gel system.

2.0 MATERIALS AND METHODS

2.1 EMBRYOS, EXPLANTS, AND MICROSCOPY

Embryos are obtained by the standard method (Kay and Peng 1991) and staged according to (Nieuwkoop and Faber 1967). Fertilized embryos are cultured in 1/3 strength Modified Barth Solution (MBS) until the desired developmental stage. Vitelline membranes are removed and microsurgery is carried out with hairloop and hair knives in Danilchik's For Amy (DFA;((Davidson, Hoffstrom et al. 2002)) supplemented with antibiotics and antomycotics to reduce contamination of explants cultures. For dorsal marginal zone (DMZ) explants that contain mesoderm, ectoderm, mesendoderm cells, embryos are selected at stage10.5 and devitelinized embryos are incised twice 90 degrees from the anterior midline (Figure 3A). Vegetal endoderm is removed along with tissues that have undergone internal involution (Davidson, Keller et al. 2004). Explants are transferred to a custom-made acrylic chamber, positioned and gently compressed with a cover slip fragment held in place with high vacuum grease (Dow Chemical). These chambers allow long term tissue culture with minimal z-drift during imaging. High resolution images of GFP tagged proteins in live tissues were collected using a 63x/1.4N.A. oil immersion lens on an inverted compound microscope equipped with a confocal scanhead (SP5; Leica Microsystems, Bannockburn IL). Capped mRNA is transcribed (Ampliscribe, Epicentre Biotech; Madison WI) from linearized expression plasmids. Approximately 0.5 to 1.0 ng of

mRNA encoding a membrane-tagged GFP (memGFP; (Wallingford, Rowning et al. 2000)), an F-actin binding GFP (moe-GFP; (Litman, Amieva et al. 2000)), and microtubule binding GFP (tauGFP; (Kwan and Kirschner 2005)) are injected at the 1-cell stage and fluorescently tagged proteins are expressed at levels that do not interfere with normal embryonic development. Images of whole embryos and explants are collected with a CCD-camera equipped stereomicroscope. Morphometric measurements are made using image analysis software (ImageJ v.1.38; Wayne Rasband, National Institutes of Health).

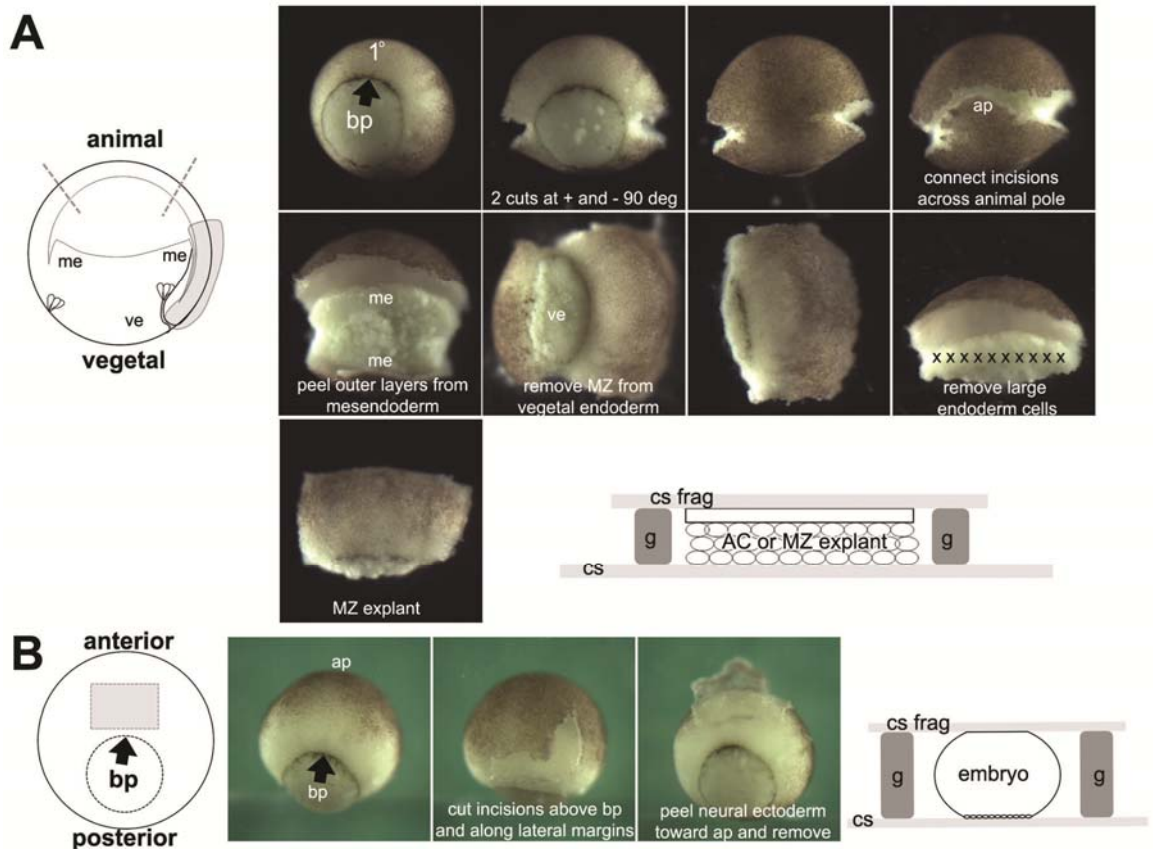

Figure 3. Microsurgery for live cell imaging

(A) Schematic representation of a sagittal cross section of an early gastrulation stage embryo (left panel). The animal cap explant is isolated through incisions along the gray dotted lines on the animal side of embryo. The MZ explant is isolated from the gray shaded area along the dorsal side of the embryo. The right-hand panel shows the individual microsurgical steps involved in isolating an MZ explant. The explant is allowed to adhere to the substrate after being held in place by a coverslip fragment bridged with silicon grease. (B) Schematic representation of the en face view of the prospective dorsal tissues of a midgastrula embryo (left panel). The "windowed" embryo is prepared by removing the gray area of ectoderm tissue from the whole embryo. The right panel illustrates the microsurgical steps required to make the windowed embryo. The window is placed face down on a large coverslip and the entire embryo is fixed in place with silicon grease and a coverslip fragment. (1°, primary blastopore lip; AC, animal cap;

ap, animal pole; bp, blastopore lip; cs, glass coverslip; g, silicone grease; me, mesendoderm; MZ,marginal zone; ve, vegetal endoderm; x x … x x, large endoderm cells.)

2.2 IMMUNOSTAINING

To fix the F-actin, fresh fixative of paraformaldehyde (4%) with glutaraldehyde (0.25%) in PBST (0.1% TritonX 100) is used. Isolated tissues or whole embryos are fixed at room temperature for 10 min to an hour, followed by F-actin stain with bodipy-FL-Phallacidin (2.5:1000) for 3hrs. Stained samples are dehydrated with Isopropanol and cleared with Murray's clear (2:1 Benzyl Benzoate to benzyl alcohol (Kay and Peng 1991) before imaging.

2.3 SMALL MOLECULAR INHIBITORS AND FLUORESCENT RECOVERY AFTER PHOTO BLEACHING (FRAP)

To modulate the F-actin polymerization state, DMZ explants are treated with LatrunculinB (0.6μM; depolymerize F-actin) or Jasplakinolide (5μM; stabilize F-actin polymerization). To increase or inhibit myosin II induced F-actin contractions, Calyculin A (CalA; a myosin light chain phosphatase inhibitor; 50n M) or Y27632 (a Rho-kinase inhibitor; 50μM) are used. These inhibitors are added in tissue culture chambers which had moe-GFP expressing DMZ explants excised from early gastrula (stages 10 to 10.5).

FRAP experiments are performed on a confocal laser scanning microscope (SP5; Leica Microsystems) with a 63X oil immersion objective with a 2X zoom. Photo-bleaching is

performed on a 7 μm by 7 μm region of cell cortex with the 488 nm argon laser operating at 100% laser power (pre- and post- bleaching images were collected with 20% laser power). Photo-bleaching is achieved using a confocal scanned pattern for approximately 5 seconds (10 iterations with 0.536 sec per scan). Fluorescence recovery is monitored for 30 additional frames at the same frame rate. Fluorescent intensity profiles over time are normalized to pre-bleach levels for each cell and analyzed with commercial curve fitting software (Matlab R2009, The MathWorks, Inc., Natick, MA) to calculate the immobile fraction of fluorophores and their characteristic recovery time (Axelrod, Koppel et al. 1976) .

2.4 DEFORMATION FIELD GENERATION USING FLEXIBLE SUBSTRATE

To visualize cell tractions generated by cells within marginal zone explants, we construct soft poly acrylamide gel substrates (FN-PAG) embedded with fluorescent beads (Leach, Brown et al. 2007). Briefly, we assemble a pre mix with final concentration of 5% Acrylamide, 0.05% Bis-acrylamide, 0.1μg/μl bovine plasma fibronectin and dark red beads (43 nm diameter FluoSpheres; Invitrogen, Carlsbad CA) in phosphate-buffered saline (PBS). The ratio of acrylamide to bis-acrylamide is chosen to produce a relatively soft gel of ~1000 Pa and confirmed by rheology tests (AR2000; TA Instruments, New Castle DE). The pre-mix solutions are deaerated for 20min to remove air from the solution, then N,N,N_,N_-Tetramethylethylenediamine (TEMED,Sigma-Aldrich), 0.01 μg/μl acrylic acid N hydroxysuccinimide (Sigma-Aldrich), and freshly made 0.4μg/μl ammonium persulfate (APS, Sigma-Aldrich) are added. Carefully mixed 4μl of pre-polymer solution is dropped on a clean cover slip and covered by a 7 by 11mm coverslip fragment. The FN-PAG is polymerized in a

humid nitrogen chamber for 30 min at room temperature. Following polymerization the coverslip fragment is carefully peeled off in 1/3X MBS solution and residual monomers are washed by exchanging 1/3 MBS 2 to 3 times. The FN-PAG is used immediately or stored for overnight in 1/3 MBS at 4°C. To visualize traction generated by mesodermal cells, we first culture the marginal zone explants on FN-PAG and collect confocal time series from cells expressing a membrane targeted GFP at the level of flexible substrate. In order to quantify cell tractions, we use registration based image analysis for displacement field generation (Sorzano, Thevenaz et al. 2005), rather than to track individual beads. Registration analysis calculates a displacement field by bringing two images into alignment, the displacement field includes both x- and y-displacements for each pixel in the original image and the distribution of traction forces can be evaluated like any intensity-based image (Russ 1999).

2.4.1 Registration-based analysis of cell- and tissue-generated traction

In order to quantify relative amounts of traction produced by cells within mesodermal tissues we adapted methods for culturing explants on force-reporting polyacrylamide gels (FN-PAG described above). Cell traction forces are often calculated from the displacements of individual beads bound within an ECM-conjugated polyacrylamide gel (Kandow, Georges et al. 2007), however, rather than track individual beads we used a method to track the displacement of parcels of gel using registration-based image analysis (Arganda-Carreras, Sorzano et al. 2006). Briefly, two-channel confocal time-lapse sequences were collected for cells within tissues expressing a membrane-targeted GFP cultured on a FN-PAG. Images of both GFP labeled cells and dark-red fluorescing beads embedded within the gel were collected at the same plane-of-focus at the top-most surface of the FN-PAG. Preliminary tests revealed that individual beads or

parcels of FN-PAG undergo periodic movements as cells appear to grab, move, and then release the gel. In order to determine the magnitude of traction forces exerted by cells within a tissue explant, we chose to measure gel displacements from the start of the time-lapse sequence rather than from a cell-free state of the gel (Beningo, Lo et al. 2002). We use the term "traction map" to refer to an image representing the absolute displacement of gel substrate produced by cells.

2.5 STATISTICAL ANALYSIS

Statistical analyses are performed with commercial software (SPSS statistics 17.0, SPSS: An IBM Company, Chicago). The correlation between two time series of cell area and moe-GFP intensities is tested by cross-correlation (Box 1976); the Pearson correlation is used to test correlations between immobile fraction and cortical actin intensity (Blalock 1972). ANOVA and T-tests are used to assess statistical differences between different drug treatments (Sokal and Rohlf 1994).

3.0 DYNAMICS OF ACTIN CYTOSKELETON

This chapter aims to examine the intrinsic dynamics of the actin cytoskeleton and reveal its role during mediolateral cell intercalation.

Most of the contents in this chapter are published in

Kim HY and Davidson LA.,(2011) Punctuated actin contractions during convergent extension and their permissive regulation by the non-canonical Wnt-signaling pathway. Journal of Cell Science; Epub ahead of print.

3.1 ACTIN CYTOSKELETON

3.1.1 Cortical actin cytoskeleton within *Xenopus* tissue

To begin to investigate the role of dynamic actin cytoskeleton during tissue morphogenesis, we first aim to show the distribution of actin cytoskeleton within isolated tissues and embryos by phalloidin staining and verify the use of the live F-actin reporter, moe-GFP. Among several approaches to report F-actin within a cell, such as injecting fluorescent G-actin (Kreis, Geiger et al. 1982) or phalloidin (Wulf, Deboben et al. 1979; Wang 1987), and expressing fluorescent F-actin binding proteins (Gerisch, Albrecht et al. 1995), we choose to use moe-GFP that was constructed with actin binding domain of rat moesin conjugated with GFP (Litman, Amieva et al. 2000). Fluorescent tagged actin binding domains have advantages of less background noise and reduced potential to alter the actin dynamics compare to other approaches.

Transverse sectioned whole embryos at mid gastrulation stage show a dense cortical F-actin layer surrounds cells where they contact either neighboring cells or fibronectin matrix (Figure 4A). F-actin is more intensely localized at tissue boundaries where fibronectin fibrils are assembled by active cellular process. Similar cortical F-actin is seen in isolated animal cap explants cultured on fibronectin coated cover glass. Reconstructed XZ projections from BODIPY-FL-Phallacidin labeled explants shows F-actin-rich protrusions on neighboring cells (Figure 4C) and concentrated F-actin ‘spots’ on the lateral surface of cells (Figure 4C’’; see arrowheads). Confocal images from moe-GFP expressing cells show structures that one

indistinguishable from F-actin structures stained with phallacidin both the cell cortex and the actin rich lammellapodia (Figure 4B and B'). In order to verify that the dynamics of moe-GFP reflected F-actin dynamics we used another live F-actin reporter, mRFP-utrophin, the mRNA encoding an RFP-tagged version of a different actin binding domain isolated from *Xenopus* utrophin (Brian M. Burkel 2007). F-actin dynamics visualized with mRFP-utrophin were similar to those observed with moe-GFP (Figure 4D and D'). Comparisons among stained and different live F-actin reporters show that moe-GFP represent the cortical F-actin within the cell cortex at the exposed surface of tissue explants as well as the F-actin localization at cell surfaces deeper in the embryo or explants.

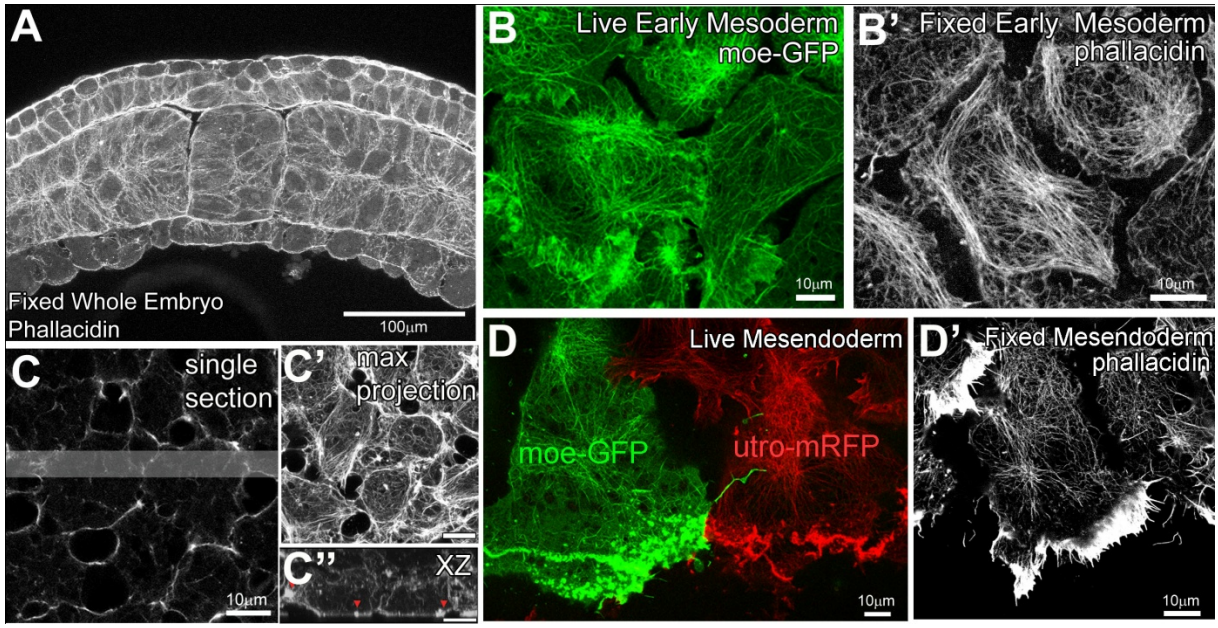

Figure 4. Cortical actin cytoskeleton within *Xenopus* tissue

(A) Maximum intensity projections of 10 μm thick confocal volumes (20 sections at 0.5 μm intervals) of F-actin stained with Phallacidin from transverse sectioned whole embryo fixed at stage 12. (B) Single confocal image of live early mesoderm cells (at stage 10.5) expressing moe-GFP. (B') A single confocal section of F-actin in fixed early mesoderm cell stained with phallacidin. (C-C'') A single confocal section of F-actin within the mid-cell body (C) within fixed animal cap ectoderm stained with phallacidin. (C') Maximum intensity projection of 3 μm thick confocal volume collected through the basolateral F-actin cortex. (C'') XZ- projection shows lateral F-actin cortex within a 23 μm thick- confocal volume from the shaded region of (C). Red arrowheads in (C'') indicate dense F-actin networks within the basolateral actin cortex. (D) Single confocal image of live mesendoderm cells expressing moe-GFP and utophin-RFP (D') A single confocal section of F-actin in fixed mesendoderm cell stained with phallacidin.

3.1.2 Altered F-actin state affects morphogenesis

To identify critical requirements for F-actin during early development we transiently disrupted the F-actin cytoskeleton. Chronic long term treatment of embryos with F-actin depolymerizing drugs such as Cytochalasin D or Latrunculin B are lethal and result in dissociation of the embryo (Kwan and Kirschner 2005). Chronic treatment precludes mechanistic studies of morphogenesis, therefore, to begin to understand the role of F-actin in morphogenesis we investigated the effect of transient inhibition of actin polymerization. We treated batches of embryos with 0.6 μM Latrunculin B (LatB; (Ilan Spector 1989)) a potent inhibitor of actin polymerization for a 20 minute period early in gastrulation and rinsed 3 times in fresh culture media and allowed treated embryos to develop. We had previously shown that brief LatB treatment dramatically reduced F-actin in whole embryos (see Figure 6A in (Zhou, Kim et al. 2009)). Embryos transiently incubated in LatB developed defects in convergent extension reminiscent of embryos defective in the non-canonical Wnt-signaling pathway including short axes and "sway-back" phenotypes (Figure 5A). The severity of convergent extension defects were dependent on the concentration of LatB (Figure 5B) and the length of treatment (data not shown). Interestingly, we did not find indications of a sensitive temporal "window" for the treatment but instead found similar phenotypes when embryos were pulsed for 20 minutes any time point during early and mid gastrulation (from stage 10 to stage 12; data not shown).

Transient reduction in F-actin polymerization had no long term effects on F-actin in embryos. The observed developmental defects do not appear to be due to long term effects on the F-actin cytoskeleton since F-actin returns to normal levels within 1 to 2 hours. Instead defects appear to result from transient rearrangements of paraxial mesoderm cells into multi-layered masses where normal paraxial mesoderm forms two distinct sheets (Figure 5C and D).

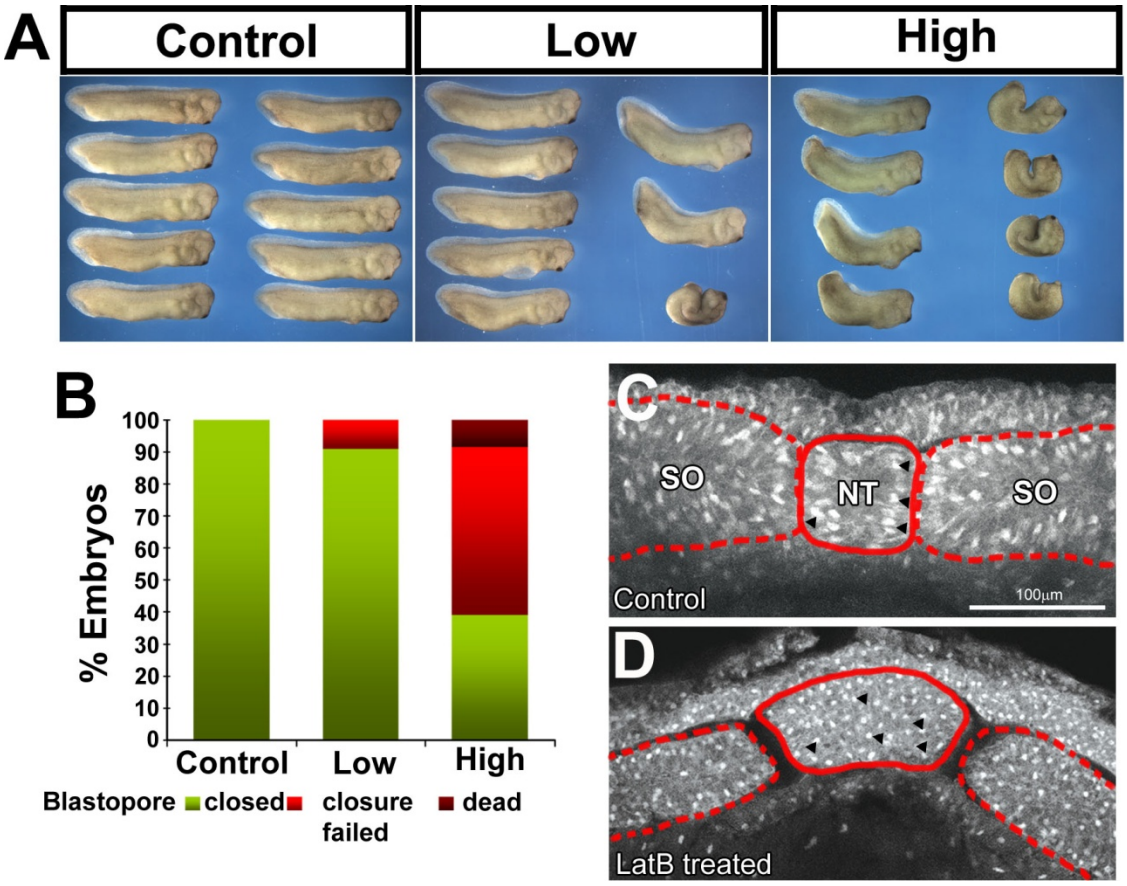

Figure 5. Transient actin depolymerization results in failure of convergent extension

(A) *Xenopus laevis* embryos were transiently treated for 20 minutes during gastrulation with low (0.6 µM) or high (1.2 µM) concentrations of Latrunculin B (LatB). LatB was washed out and whole embryos cultured until they reached tadpole stages. Embryos exposed to a pulse of LatB during mid-gastrulation developed short and bent axis by a dose dependent manner. (B) Blastopore closure defects increased with the concentration of LatB. (C) Transverse sectioned dorsal tissue of control embryos show ordered positioning of nuclei within two cell layers in mesoderm (arrowheads). (D) Three hours after the LatB pulse-wash, dorsal tissue has randomly positioned rounded cells in multiple layers that thicken both the ectoderm and mesoderm. Cell shapes are visualized by rhodamine-Dextran injection at single cell stage. (so - somite, nt - notochord)

3.1.3 F-actin dynamics and cell behaviors

The result from transient disruption of actin polymerization supports the essential role of dynamic actin cytoskeleton and suggests further inspection of the relationship between cortical F-actin dynamics and cell behaviors during cell rearrangements. We expressed moe-GFP to visualize the F-actin and prepared the windowed embryo (see Figure 3B) that retains the closest environments that mesoderm cells experience during the cell intercalation within embryo. By collecting dual depths of confocal sections either at F-actin cortex or cell body for time-lapse imaging, we were able to follow their dynamics simultaneously. Exposed mesoderm cells from the live embryo have complex F-actin network under the cell membrane and the actin network exhibits remarkable dynamics (Figure 6A). To assess whether there is a link between actin contractions and cell shape changes, we monitored the changes of average moe-GFP intensities and area of the cell. As moe-GFP intensity increases the cell area decreases. The mesoderm cells deform their neighbors easily (Figure 6A') and we find changes in cortical actin contractions are significantly correlated with changes of cell shape (Figure 6B and C; cross correlation coefficient is -0.89 in the marked cell in A, and mean value is -0.76 from 12 cells of three time-lapse movies). We conclude that cortical actin contractions are directly involved in cell behaviors yet we need further study to identify the consequence of the events.

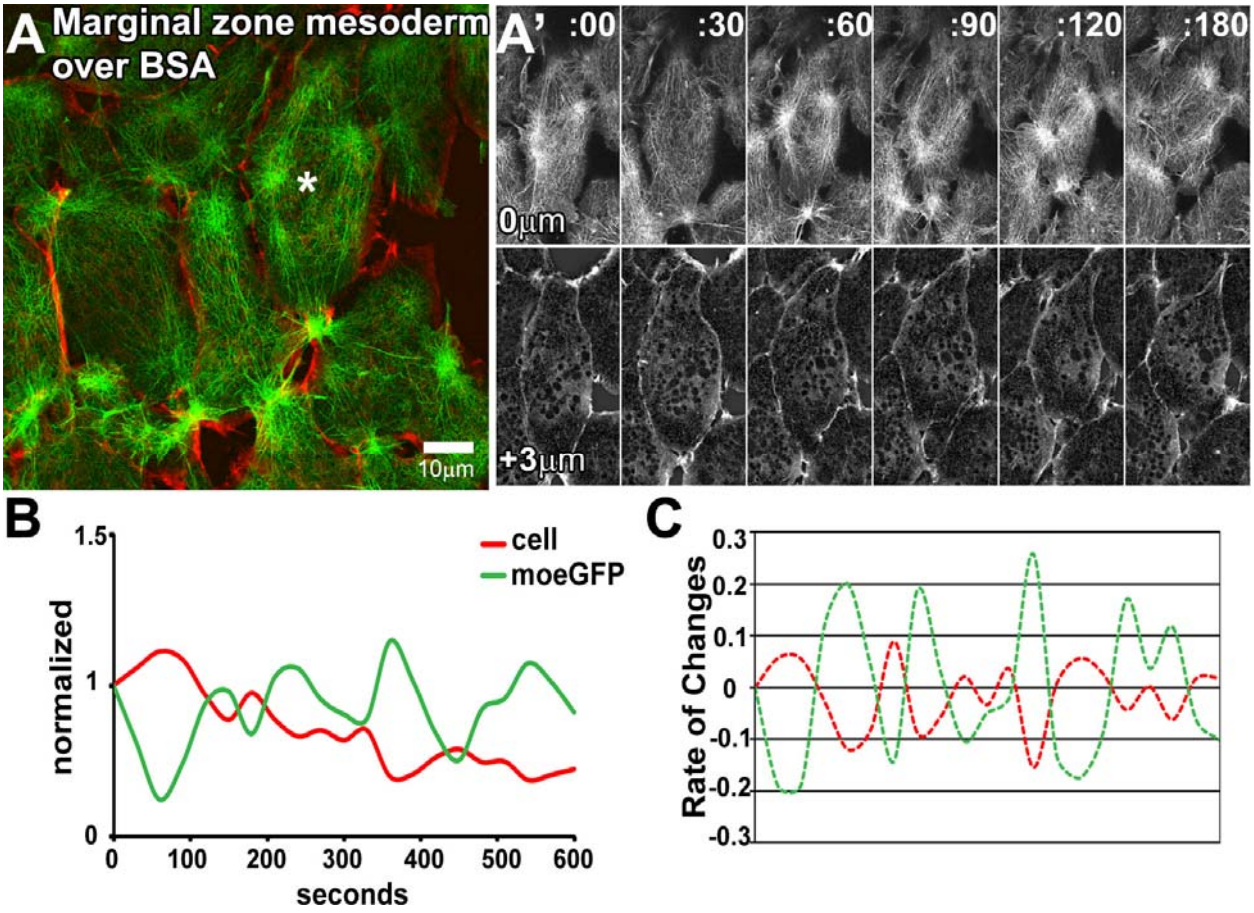

Figure 6. Cortical actin contractions are correlated with cell behaviors

(A) Dual depth of confocal sections were taken either for F-actin cortex (green) or for cell outline (red) to capture the dynamics of both cell behaviors and F-actin with moe-GFP expressing marginal zone mesoderm from the windowed embryo. (A') Time sequences from (A) time-lapse of marked cell. (B) A cell area is inversely correlated with moe-GFP intensities from the cell (from marked cell in (A)). Area of the cell decreases (or cells contract their body) as moe-GFP intensity increases (or F-actin network get tensed). (C) Rate of changing the cell area and moe-GFP intensities parallels over time. The mean cross correlation coefficient for the rate of changes between cell area and moe-GFP intensity is -0.76 (12 cells from three time-lapse movies).

3.1.4 F-actin dynamics in various microenvironments

Our observation of complex F-actin structures and contraction dynamics (Figure 4 and 7) lead us a series of questions about consequences of the microenvironment and developmental stages of embryos on the dynamics of actin contractions. First, since embryonic tissues cultured fibronectin substrates that can limit large scale cell movements, we wondered whether cortical actin contractions occurred in cells cultured on non-adhesive substrates and whether individual F-actin contractions could alter cell shapes. To separate effect of substrate adhesion from cortical actin contractions, we provide non-adhesive substrates such as agarose or bovine serum albumin (BSA) coated cover glass (Figure 6 and 8). When cultured on a non-adhesive substrate, cells within a microsurgically isolated tissue (Figure 7) and cells within a "windowed" whole embryo (Figure 6) show similar F-actin dynamics as cells cultured on a fibronectin substrate (Figure 10). The external substrate-free environment enables cells to deform their neighbors more easily and we find cortical actin contractions are significantly correlated with changes of cell shape (Figure 6). Similar observations of actin or myosin regulatory light chain dynamics and their effect on cell shape have been reported during epithelial morphogenetic movements in Drosophila (Martin, Kaschube et al. 2009; Blanchard, Murugesu et al. 2010) but have not been observed in during vertebrate morphogenetic movements. We conclude that punctuated actin contractions generate sufficient force to deform cells in the embryo, but have a more limited effect when cells are more firmly bound to fibronectin-coated substrates.

Next, we wondered whether cell-cell contact in embryonic tissues induced the actin contractions. To investigate this question we dissociated mesoderm cells from MZ explants with Ca^{++}/Mg^{++} free DFA, moved the cells back to DFA, and cultured them on a fibronectin substrate. On fibronectin we found single cells as well as two- and three-cell clusters (Figure 7). Although

cell clusters had denser F-actin arrays than single cells, we could easily observe F-actin contractions within both populations. In addition, cortical actin contractions can be found throughout the embryo, in ventral mesoderm cells from isolated explants, and animal cap cells as early as the mid-blastula transition (Figure 7).

Therefore the use of substrate-free culture and observation of F-actin contractions within dissociated cells confirmed the importance of cortical F-actin contractions in guiding cell shape changes, while the cortical actin contractions are the common feature within embryonic tissue. For the remainder of this dissertation we use explants cultured on fibronectin since cell behaviors are well characterized in these explants and the actin cortex is optimally positioned for confocal imaging.

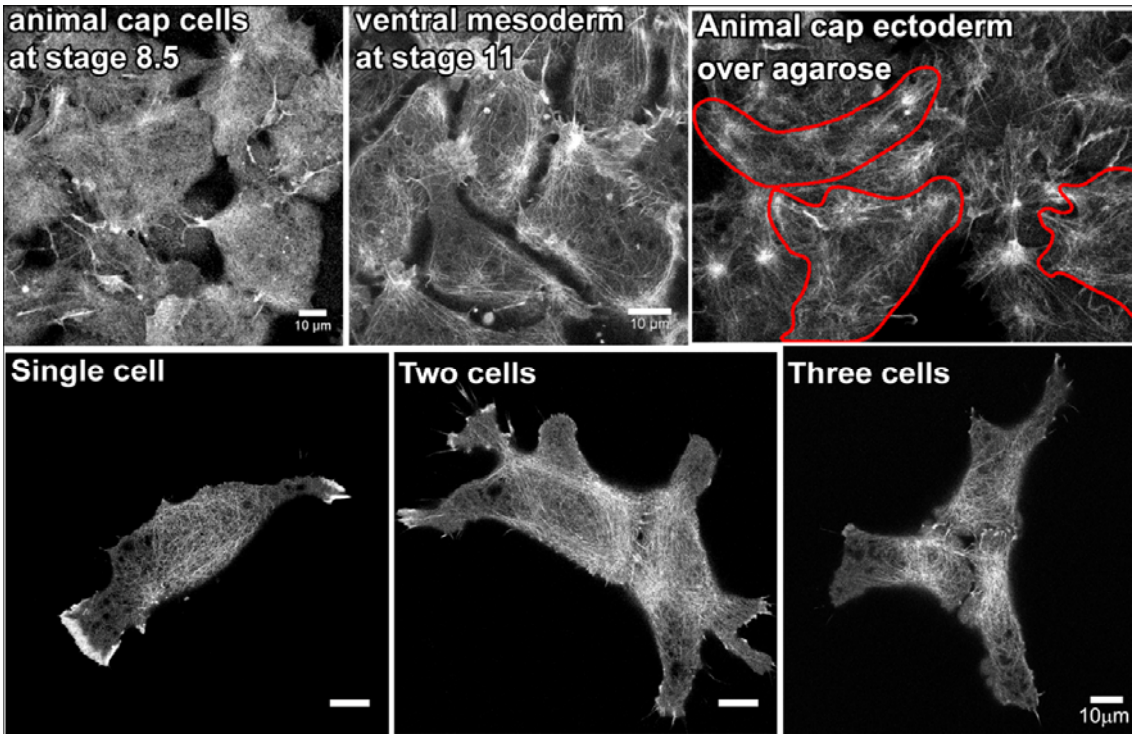

Figure 7. Cortical actin contractions in various microenvironments

F-actin contractions found ubiquitously throughout the embryo and exhibit similar F-actin network and dynamics as cells in marginal zone explants. Scatter labeled moe-GFP expressing early animal cap ectoderm cells (Stage 8.5), ventral mesoderm cells (Stage 11), and animal cap ectoderm cells over agarose. (Note: early animal cap ectoderm has faint levels of moe-GFP labeling F-actin.). Confocal images of moe-GFP from dissociated mesoderm cells cultured on fibronectin coated cover glass.

3.2 ANALYZE THE DYNAMICS OF CORTICAL F-ACTIN CONTRACTIONS

To investigate live actin dynamics during tissue convergence and extension we injected moe-GFP mRNA at one cell stage, prepared marginal zone explants at early gastrula stage (stage 10), and culture on the fibronectin coated cover glass. High resolution time-lapse imaging of F-actin allowed us to observe dynamics of F-actin within cortex of cell body in addition to dynamics within lamellpapodial actin networks. We found the F-actin network undergoes a cycle of contraction and relaxation within a part of cell body that increases in density as F-actin gathers in a focal point and dissipates over time (Figure 8). We called these F-actin dynamics as 'punctuated actin contraction'. Since this unique actin dynamics seems to occur within most cell populations in embryos including ectoderm, mesoderm, and mesendoderm within marginal zone explants (Figure 10), and closely related to the cell behaviors (Figure 6), we investigated methods to quantify the punctuated actin contractions from confocal time-lapse images.

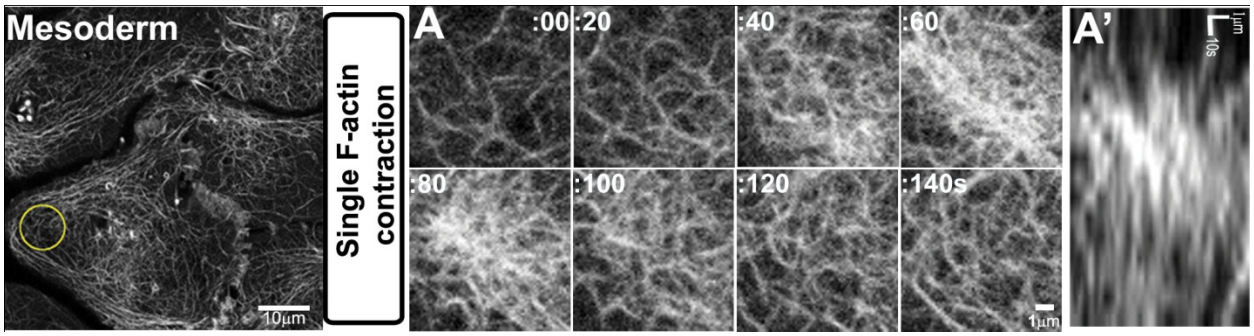

Figure 8. The punctuated actin contraction

Confocal images of moe-GFP expressing early mesoderm cells in dorsal marginal zone (DMZ) tissue. (A) A time series of confocal images of a single cortical F-actin contraction within an early mesoderm cell (circled region). (A') Kymograph of intensities through the mid line of the same contraction as in (A).

3.2.1 Fixed selection

As a first attempt to quantify dynamics of the punctuated actin contractions, we measured the moe-GFP intensities over time for the selected circular region of actin cortex. This approach allowed us to characterize the formation of F-actin contractions, however, these qualitative methods could not adequately describe the physical dynamics of the punctuated F-actin contractions or suggest how these structures might be controlled or localized. However, we could identify few number of punctuated actin contractions at the fixed selection of actin cortex for short sequences from the collected time-lapse movie. Interestingly we found that four different cell types including ectocerm, early mesoderm, late mesoderm, and mesendoderm cells, share a similar pattern of kinematic on accumulation and dissipation (Figure 9). The changing intensity of the F-actin network over a single episode of contraction typically last form 60 to 120seconds even the maximum intensity of each contraction varies. In addition, the rate of accumulation is clearly higher than the rate of disassembly (Figure 9).

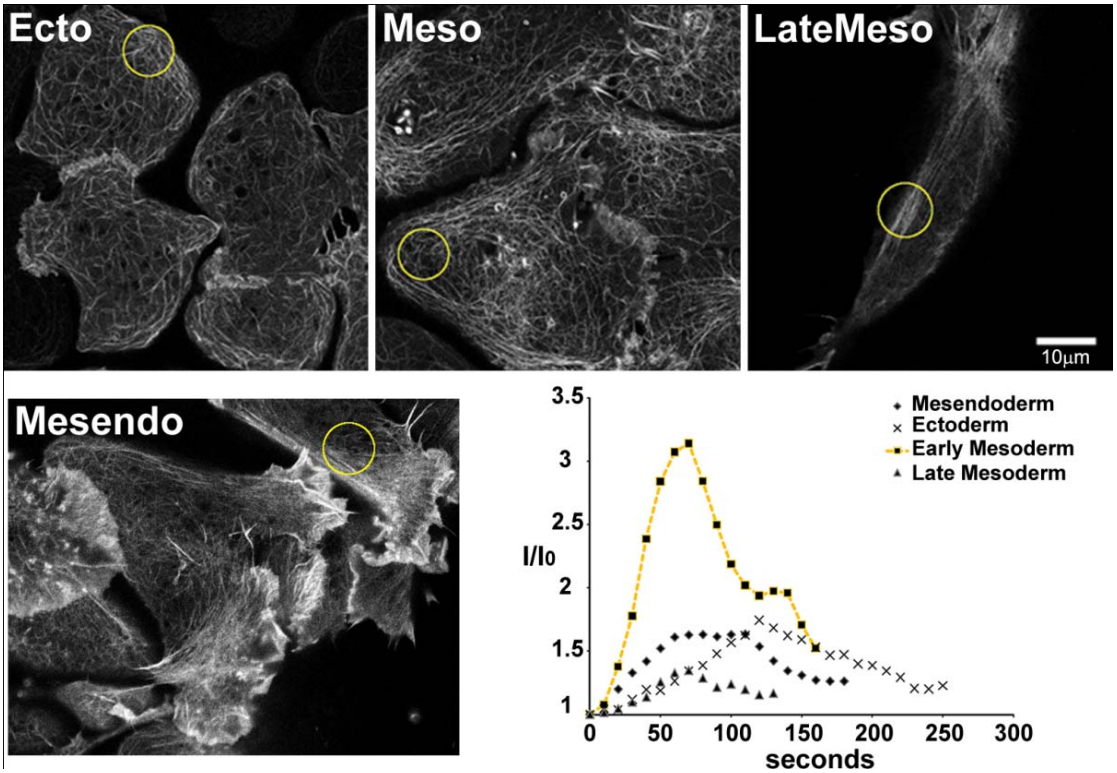

Figure 9. Punctuated actin contractions within dorsal marginal zone tissue

Confocal images of moe-GFP from cells in dorsal marginal zone (MZ) tissue including mesendoderm, ectoderm, early mesoderm, and late mesoderm cells. Moe-GFP intensity profiles in circular region of cells for one episode of F-actin contraction. Normalized intensity (I/I_0; initial intensity - I_0) within a circular region of each cell type (circles in scatter-labeled cells in MZ) over a single contraction.

3.2.2 Dynamic selection

To get a better understanding of the complex dynamics of punctuated actin contractions, we modified the quantification approach to track assembly dynamics as well as follow contraction movements. To investigate the temporal and spatial dynamics of the punctuated F-actin contractions which form moving structures akin to unitary sites of focal adhesions, we adapted image processing tools appropriate to tracking discrete objects in cells (Figure 10A). In order to detect fluctuations of F-actin intensity over time within the mid-cell cortex and to track dynamics of the individual punctuated F-actin contraction event, first mid-body region within the cell is manually selected from a single frame in the 10 minute confocal time-lapse sequence. The selected region of interest contains the cell mid-body and excludes lamellipodia and cell-cell contacts (ROI-Cell). The ROI-Cell is then subdivided into small hexagonal units; ROI-hexagon is 2.4 μm diameter containing approximately 270 pixels. The hexagonal shape has been chosen to register the presence of multiple actin filaments or bundles and track these cytoskeletal elements as a contiguous structure once the F-actin network contracts. To classify the status of the F-actin within the hexagon we compared the F-actin intensity within the hexagon to the mean intensity within the ROI-Cell. In the first round of analysis, hexagons are classified as a "contraction-active" if the F-actin signal intensity within the ROI-hexagon is greater than 150% of the mean intensity of ROI-Cell. At this stage in the analysis each contraction-active hexagon represents a small patch of contracted F-actin cortex within a single image (Figure 10B).

Since F-actin contractions may extend over large areas of the cell, can persist for several minutes, and change shape, we extended the classification scheme to connect multiple contraction-active hexagons within a time-lapse sequence. First, we developed a decision flow chart to assign ROI-hexagons into multi-hexagon patches within the same frame. Next, we

extended the flow chart logic to bridge small temporal gaps in the history of a single hexagon over the course of a single punctuated F-actin contraction. In brief, in order for an ROI-hexagon to be included in a punctuated F-actin contraction: 1) a contraction must be seen in three contiguous hexagons, 2) persist for at least 30 seconds, and 3) to be counted as the same event, multi-hexagon contractions must overlap from frame to frame. Given the stringent contraction-threshold of 150%, we merged single transiently non-contractile hexagons into punctuated contractions if they were completely bounded by contractile hexagons. This segmentation process allowed us to identify and track high density regions of F-actin cortex (Figure 10E, E', and E'') from the formation of a contraction to the end providing information on how punctuated F-actin contractions moved as they formed, spread, and contracted.

In addition to tracking formation and movements of single contractions our analysis measured the frequency of punctuated contractions within the mid-cell cortex and identified sub-cellular domains where multiple contractions occurred. Contractility within a cell can be reported as a contractile area (Figure 10C) or displayed in an F-actin contraction frequency map (Figure 10D). Contractile area is defined as the total area covered by punctuated contractions over the course of the time-lapse (analogous to the Boolean "OR"). In contrast to the morphological identification of multi-hexagon contraction events, the frequency map represents the chances of finding contractile F-actin within each hexagon. To highlight relative levels of F-actin contractions within a cell cortex, the F-actin frequency map calculates the average "contractility" for each ROI-hexagon in the ROI-Cell. The frequency map tracks the chance of contraction within any particular hexagon. Orientations of punctuated F-actin contraction movements are measured with respect to the cell major axis (Figure 10G) and plotted in a circular histogram (see Figure 11 d',e' and f'). This image analysis procedure allows us to quantify punctuated F-actin

contraction life-time, frequency, and movements and to compare and contrast these features of F-actin dynamics across a variety of cell types, developmental stages, and treatments.

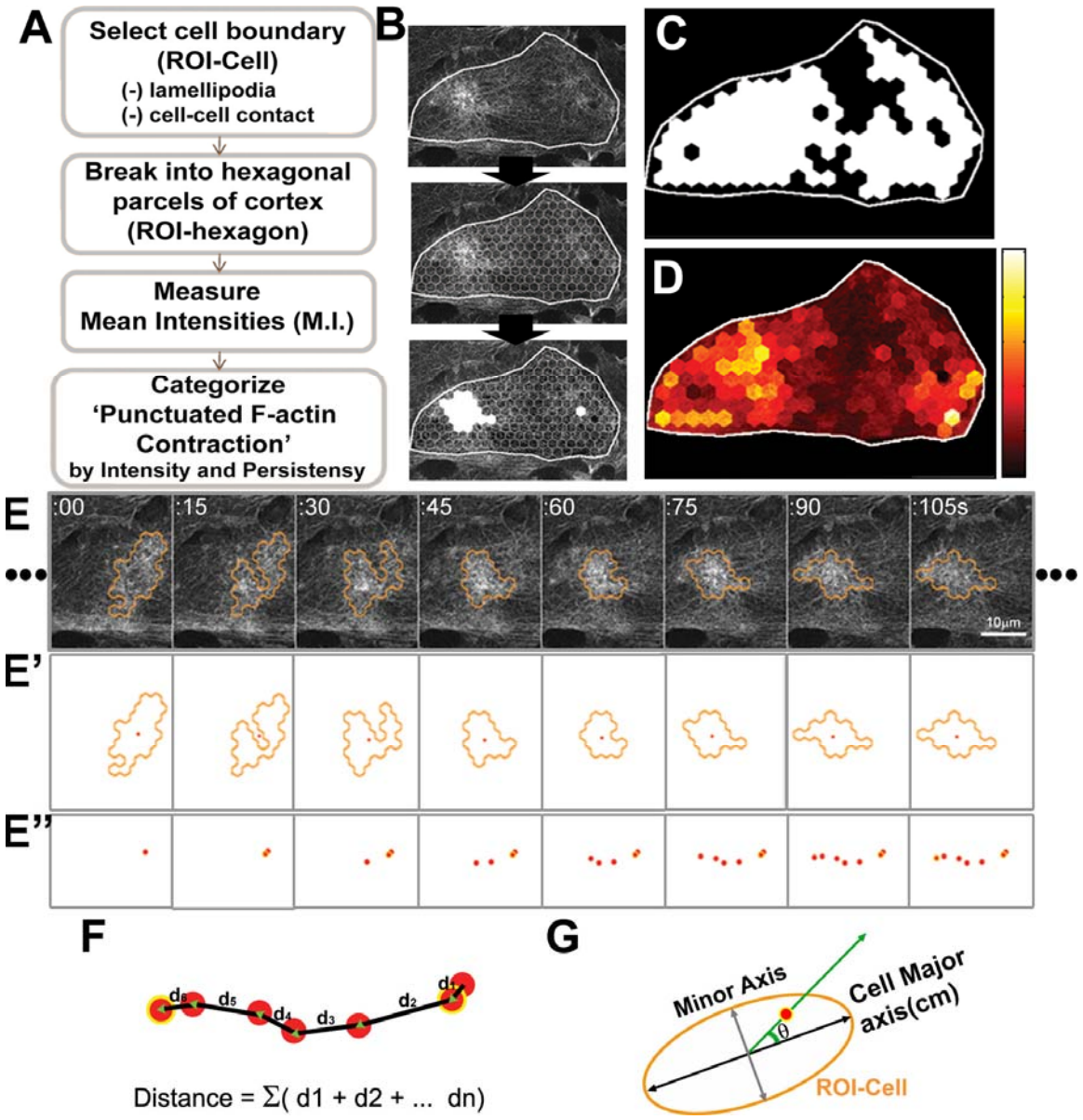

Figure 10. Quantitative approaches to analyze the punctuated F-actin contractions

The shape, duration, and movement of individual puncutated F-actin contractions are quantified based on local and global intensity changes of F-actin within cell cortex. (A) Flow chart for image processing steps to identify the contractile actin cortex and categorize the individual 'punctuated F-actin contraction' (B) Subdivision of a moe-GFP labeled cell into the cell boundary (ROI-Cell) in white line, divided hexagonal parcels (ROI-hexagon) within the boundary, and identified "active" actin cortex with white filled-ROI-hexagons. (C) The contractile area displays the place that dynamic F-actin cortex stayed over 30mins. (D)

The incident frequency of F-actin contractions in each ROI-hexagon is shown by the F-actin frequency map. Frequency is scaled with hot psuedo-color and highlights the relative occurences of active F-actin cortex. (30 minute time-lapse used for (C nd D)) (E) Following identified punctuate F-actin contraction in time-lapse movie of moe-GFP. (E'-E'') Identified positions (red dots) by center of intensity of categorized actin contraction enclosed by hexagonal area. (F) Distance of movements is sum of segmented distances for one episode of F-actin contraction. (G) Anglular distributions of positions of F-actin contractions in respect to the major cell (cm) axis represented by angle θ. The heat-map colors in (D) indicate an arbitrary frequency scale from high frequency "light" to low frequency "dark".

3.3 DYNAMICS OF PUNCTUATED ACTIN CONTRACTIONS DURING CONVERGENC AND EXTENSION

Since mesodermal cell shapes progress from isodiametric to mediolaterally elongate over the course of convergent extension, we wondered whether cortical F-actin dynamics are also varying in different cell types and developmental stages. To examine correlations of the punctuated F-actin contractions to distinct cell behaviors, first we compared the pattern of punctuated F-actin contractions using frequency maps constructed from 10 minute duration confocal time-lapse sequences of moe-GFP collected from different regions within marginal zone explants (Figure11- a, b, and c, respectively from ectoderm, early mesoderm, and late mesoderm cells).

We found very different frequency maps among cell populations. Small patches of intermediate intensity hexagons along the edge of ectoderm cells show these regions contain fewer F-actin contractions (Figure 11a) in contrast to early mesoderm cells which include a large number of F-actin contractions (Figure 11b). The frequency of contractions in late mesoderm cells display an equally distinctive pattern, forming highly persistent F-actin contractions running

parallel to the major cell axis (Figure 11c). Since both punctuated contractions and lamellipodial protrusions aligned to the cell we thought punctuated F-actin contractions might play a role in elongating mesoderm cells.

To investigate the role of punctuated contractions in shaping cells and whether the movements of individual F-actin contractions could account for patterns in the frequency map, we tracked contraction positions as they formed, moved and disappeared. Trajectories of the movement of the centers of punctuated contractions from one representative cell in each population shows that contractions can move either randomly or in distinct patterns (Figure 11-d, e, and f). The infrequent contractions within ectoderm cells move in random directions and do not move far from their initial site of formation (11.42 ± 7.38μm per contraction; 17 cells). In contrast, the centers of punctuated F-actin contractions move larger distances in both early (18.50 ± 21.03μm per contraction; 17 cells) and late mesoderm (18.49 ± 25.62μm per contraction; 14 cells).

Movements of punctuated F-actin contractions in mesoderm cells change during gastrulation. In late gastrula mesoderm cells, individual punctuated F-actin contraction appear to move back and forth, oscillating along the same path, whereas in early mesoderm and ectoderm cells they move randomly (Figure 11 d, e, and f). Since mesoderm cells elongate from early to late gastrula stages, we suspected the orientation of punctuated F-actin contraction movements were related to the elongation of the cell. To test our hypothesis, we measured length-to-width ratio (LTW) of cells and the angle (θ) of F-actin contractions with respect to the major axis of the cell. Even though some early mesoderm cells elongate to LTW greater than 2, we found movements of punctuated F-actin contractions align to major cell axis only in late mesoderm cells (Figure 11 d', e', f '; Figure 12). In contrast, punctuated F-actin contractions do not move

parallel to the long cell axis in either ectoderm or early mesoderm cells. These results indicate that individual punctuated F-actin contractions move along the major cell axis only within late gastrula mesoderm cells

Thus, the frequency and movement of punctuated F-actin contractions are developmentally patterned across populations of cells in marginal zone explants. Ectoderm cells have random and infrequent contractions. Early mesoderm cells have frequent contractions which move randomly. Late mesoderm cells have frequent contractions whose movements are oriented with cell shape. Additionally since increased frequency and progressively oriented movements of the punctuated F-actin contractions coincide with cell shape changes we suspect punctuated F-actin contractions play an important role in regulating cell behaviors during convergent extension of the *Xenopus* mesoderm.

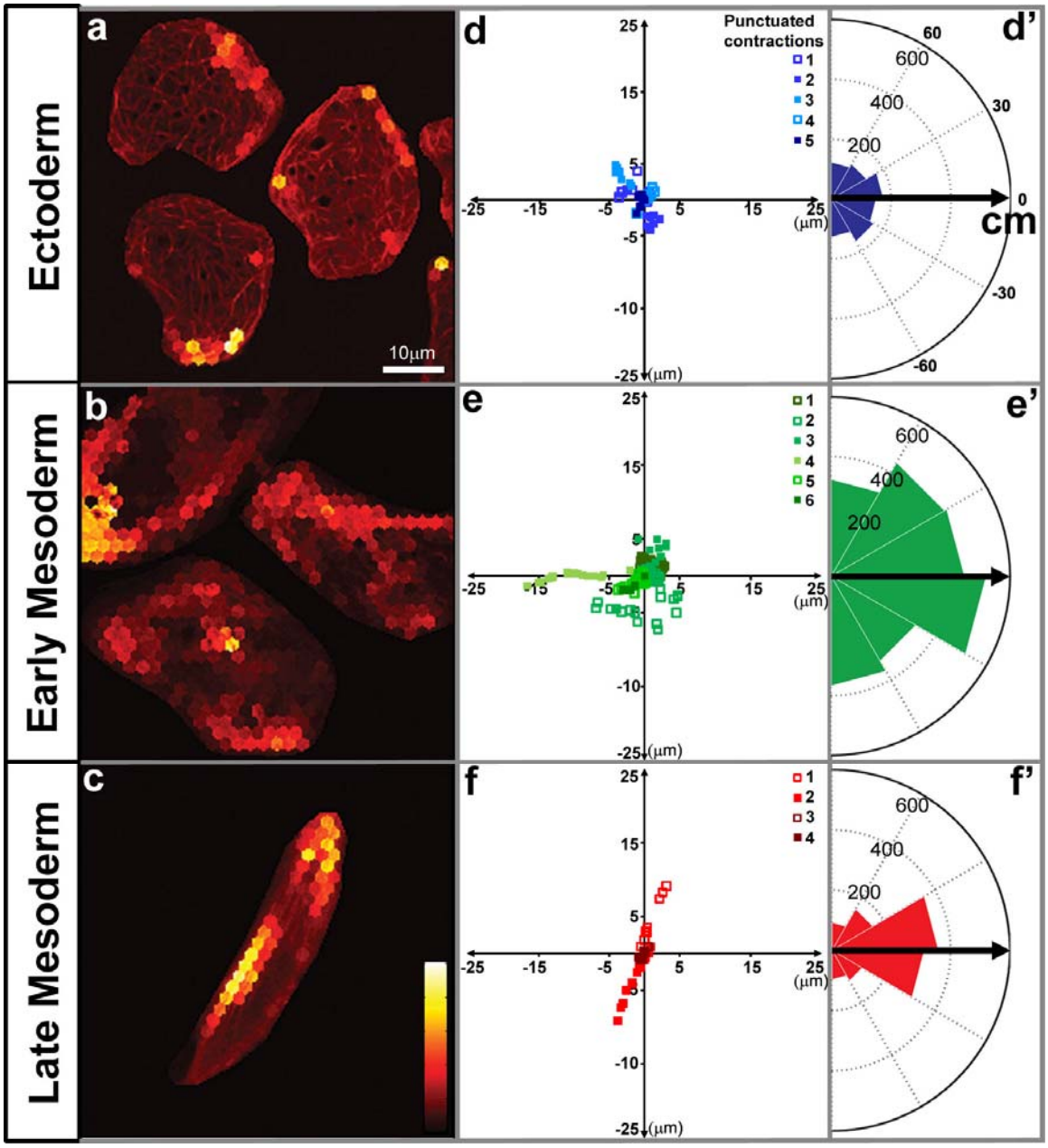

Figure 11. Punctuated F-actin Contractions within DMZ

(a-c) F-actin frequency maps from confocal time-lapse of moe-GFP expressing ectoderm (a), early mesoderm (b), and late mesoderm (c) cells. (d-f) Scatter plots display relative walking positions of punctuated F-actin contractions from one representative cell starting from its origin (0,0). (d'-f') Circular histograms represent angular distribution of punctuated F-actin contractions with respect to the cell major axis (cm).

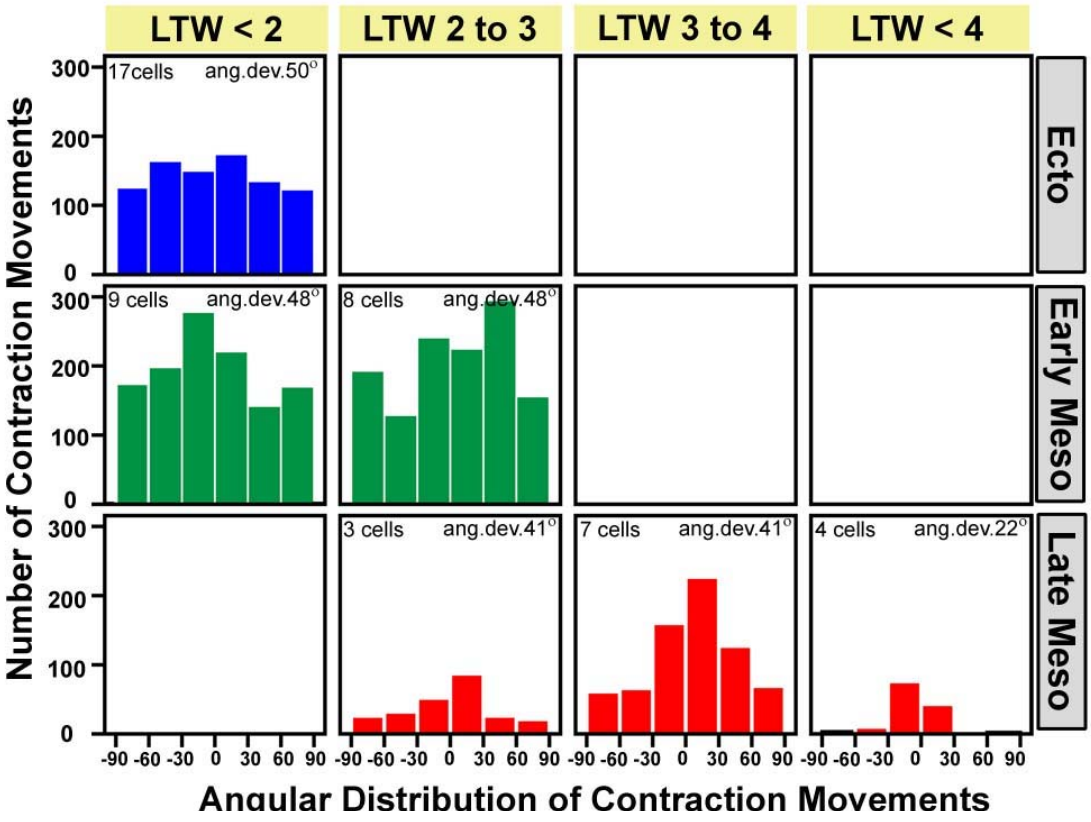

Figure 12. Further analysis of angular distribution of punctuated actin contraction movements

The angular distributions of punctuated actin contraction movements from Figure11 are binned by the length-to-width (LTW) ratios of cells in ectoderm, early mesoderm, and late mesoderm. The frequency reports the number of motion segments of tracked punctuated actin contractions oriented within each angle bin. For each stage (ectoderm, early mesoderm, late mesoderm), the frequency was binned by the length-to-width-ratio of the cells (below 2, 2 to 3, 3 to 4, and above 4). The angular deviation for each distribution is indicted for each plot. Actin contractions are not oriented to the cell axis in moderately elongated early mesoderm cells (LTW from 2 to 3) compared to equally elongated late mesoderm cells. The cell major axis is oriented by convention at 0°. (Note: ang.dev. is the angular deviation of the circular distribution and is equivalent to the standard deviation calculated for linear data (Zar 1998))

Table 1. Quantified dynamics of punctuated F-actin contractions in DMZ

(Mean ±STD)	Ectoderm	Early mesoderm	Late mesoderm
# of explants	6	6	6
# of cells	17	17	14
Cell shape (LTW)	1.45±0.23	1.91±0.47	3.69±1.15
Contractile area (%)	20±13	45±9	35±11
Rate of contractions (#/hr)	15.90	45.94	46.71
Life span (min) per Contraction	3.24±2.48	3.11±2.57	2.42±1.98
Distance (μm) per Contraction	11.42±7.38	18.50±21.03	18.49±25.62

3.4 CONCLUSION AND DISCUSSION

Cells in developing *Xenopus* embryos contain a complex and dynamic F-actin-rich cortex that is closely correlated with cell behaviors. Transient disruption of the actin cytoskeletal networks during gastrulation results in permanent defects in morphogenesis. To describe this F-actin network during morphogenesis we use moe-GFP to label tissues for live-confocal imaging and adapt quantitative image analysis approach. We find rapidly moving F-actin features, referred to here as punctuated F-actin contractions, within the cell cortex, and then compare contraction dynamics in different cell types. Different cells exhibit distinct patterns of F-actin contractions. Static and less frequent punctuated F-actin contractions are present in ectoderm cells. Contractions are more frequent in mesoderm cells and translocate over larger distances than contractions in ectoderm. Furthermore, contractions in early mesoderm and ectoderm are randomly oriented but switch to move parallel to the cell's longest axis at later gastrula stages.

Our observation allows us to draw parallels between the role of actomyosin in regulating motility in single cells or in coordinating morphogenesis in convergent extension. Actomyosin dynamics play essential roles in cell spreading (Senju and Miyata 2009), polarized cell migration (Yam, Wilson et al. 2007), and the establishment and maintenance of adherens junctions (Liu, Tan et al. 2010; Smutny, Cox et al. 2010). The events of single episodes of punctuated F-actin contractions are shared among many different cell types in *Xenopus* embryos, however, the frequency, localization, and movements are not. For instance, contractions switch from randomly oriented movement to mediolaterally aligned movement as mesodermal cells elongate parallel to the mediolateral axis. We suggest several ways that altered patterns of F-actin contraction might change cell shapes. First, aligned contractions might serve to reinforce the movement of a cell in the direction of contraction or mediolateral aligned contractions might allow mesodermal cells to

better resist externally applied forces that would elongate the cell. Excessive mediolateral cell elongation could reduce the efficient conversion of mediolateral cell intercalation to convergent extension. An alternative function for contractions might be to enhance the rate of intercalation. Cycles of contraction aligned to the mediolateral axis could operate in a ratchet-like fashion with cycles of cell adhesion to drive mediolateral cell intercalation. Neither of these two mechanisms is mutually exclusive and oriented F-actin contractions could serve both functions.

4.0 NON-CANONICAL WNT-SIGNALING PATHWAY REGULATES PUNCTUATED ACTIN CONTRACTIONS

This chapter aims to investigate the role of non-canonical Wnt-singling pathway in regulating the dynamics of punctuated F-actin contractions during mediolateral cell intercalation.

Most of the contents in this chapter are published in

Kim HY and Davidson LA.,(2011) Punctuated actin contractions during convergent extension and their permissive regulation by the non-canonical Wnt-signaling pathway. Journal of Cell Science; Epub ahead of print.

4.1 FAILURE OF CONVERGENT EXTENSION FROM ALTERED NON-CANONICAL WNT-SIGNALING PATHWAY

Since punctuated F-actin contractions regulate cell shape change and the actomyosin network is a downstream target of the non-canonical Wnt-signaling during the convergent extension of frog embryo, we are interested in role of Wnt-signaling in modulating these actin contractions. To investigate the role of non-canonical Wnt-signaling on the punctuated actin contractions, first we examine the phenotypes of embryo, dorsal marginal zone explants, and mesoderm cells within the explants that altered the signals through over expression of extracellular, transmembrane and intracellular proteins respectively, dominant negative Wnt (dnWnt), Frizzeld7 (Xfz7), and the mutant form of disheveled protein (Xdd1). At four cell stage, 1-2 ng of mRNA were injected into dorsal animal blastomeres. To locate the cells are expressing these mRNAs, we often co-injected them with fluorescent protein conjugated dextran or membrane binding proteins.

Embryos expressing dnWnt, Xdd1, and Xfz7 consistently showed the phenotype defects consisting of shortened anterior–posterior axes and failure in neural tube closure (Figure 13; data only shown for dnWnt expressing embryos). Similar neural tube closure defects occurred within dnWnt expressing dorsal marginal zone explants which have a broader notochord region with round mesoderm cells. In contrast, control explants have a narrow notochord region with elongated mesoderm cells (Figure 13; see red arrow heads). These phenotype results of embryo and explant, confirm that we can consistently reproduce the previous findings (Wallingford, Rowning et al. 2000), and therefore continue to explore the effects on actin cytoskeleton.

To account for the possibility that over-expression of non-canonical Wnt-signaling proteins alter levels of endogenous F-actin, we used bodipy FL-phallacidin to visualize F-actin in whole embryos. Xdd1 and Xfz7 over-expression does not affect overall F-actin levels seen in transversely bisected whole embryos (Figure 14). Normal levels of F-actin can be seen in round Xdd1 and Xfz7 expressing cells mixed with control cells in the notochord and neural ectoderm where disorganized cells form multi-layered tissue (Figure 14; see arrows). However the multi-layered notochord tissue has the similar phenotypic changes that had been shown with transient actin depolymerization (see Figure 5C and D), suggesting that the morphogenesis defects are caused by altered dynamics of actin cytoskeleton.

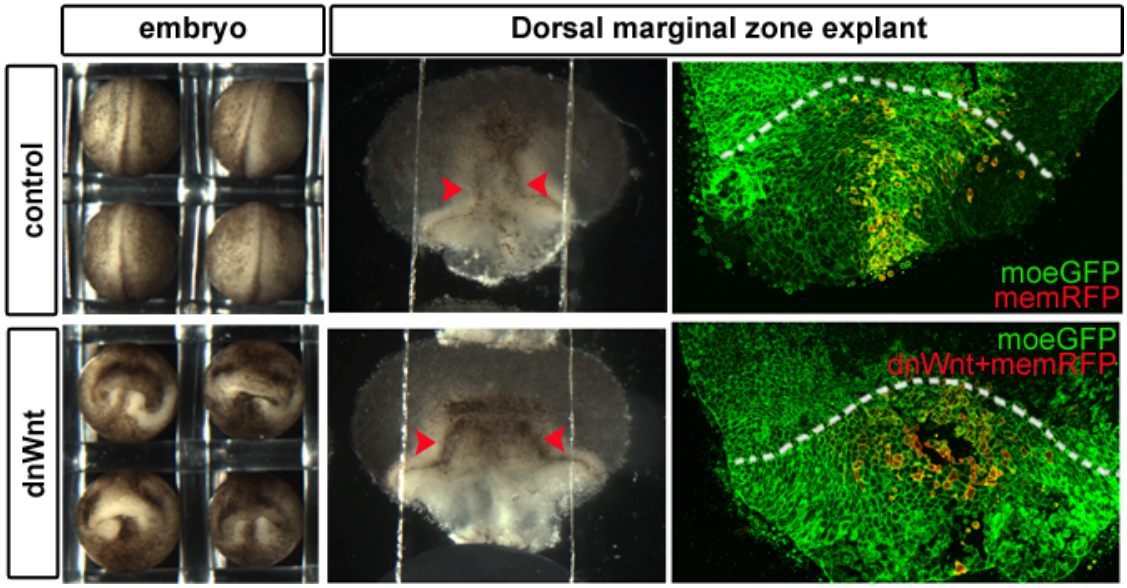

Figure 13. Blocking non-canonical Wnt-signaling cause failure of convergent extension

Control and dnWnt expressing embryos and dorsal marginal zone explants. dnWnt expressing embryos have broad notochord regions and failed neural tube closure (at stage 16.5). dnWnt expressing cells (red cells) are isodimetric compare to elongated mesoderm cells in control explants.

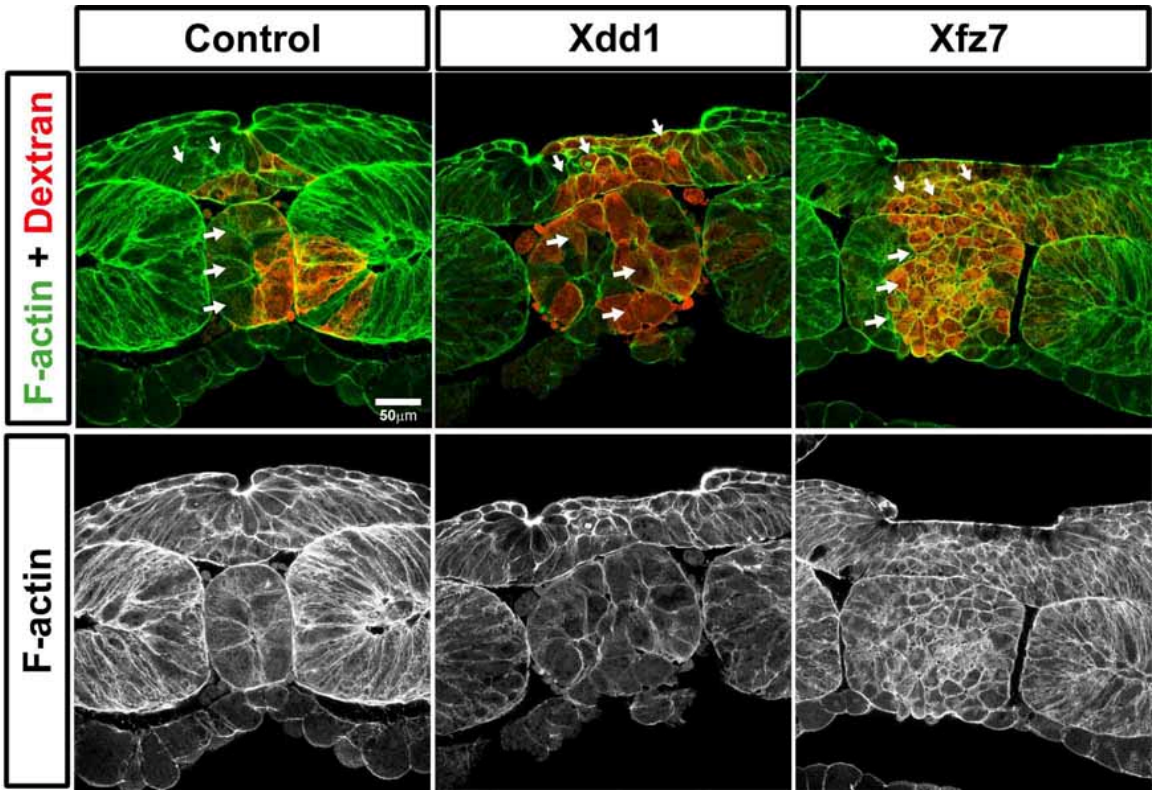

Figure 14. Defects in non-canonical Wnt-signaling cause multi-layering of tissues

Maximum intensity projections of 5µm thick confocal volumes show Bodipy-FL Phallacidin stained F-actin cortex from transversely bisected whole embryos at stage 16.5. Embryos have similar levels of F-actin cortex in control, Xdd1, and Xfz7 expressing cells, but altered non-canonical Wnt-signaling results in multi-layered cells in notochord and neural plate tissue. Both Xdd1 and Xfz7 expressing embryos have open neural plates with two widely spaced hinge points. 70kd Rhodamine-Dextran co-injected with Xdd1 and Xfz7 mRNA identifies cells expressing these mRNAs within the embryo. Control embryos are only injected with Rhodamine-Dextran.

4.2 ROLE OF NON-CANONICAL WNT-SIGNALS ON PUNTUATED ACTIN CONTRACTIONS

The non-canonical Wnt-signaling pathway controls mediolateral polarity of mesoderm cells during convergent extension in *Xenopus* by activating RhoGTPases which in turn modulates the actin cytoskeleton (Habas, Kato et al. 2001). It is thought that a Wnt-signal activates a Fz receptor which translocate Dsh to the plasma membrane (Wallingford, Rowning et al. 2000) to promote RhoGTPase activation (Habas, Dawid et al. 2003). To investigate the role of the non-canonical Wnt-signaling on actin contractions we chose to alter signals from either Fz receptor or Dvl cytoplasmic protein. In addition, we co-injected moe-GFP mRNA and Xdd1 or Xfz7 mRNA and collected confocal time-lapses from moe-GFP expressing cells within marginal zone explants to follow F-actin dynamics in live cells during gastrulation.

4.2.1 Altered actin contractions with Frizzled7

Since Xfz7 is expressed by involuting mesoderm cells during gastrulation and mediate mediolateral intercalation cell behaviors (Djiane, Riou et al. 2000), we hypothesized that we could activate punctuated actin contractions by expressing Xfz7 in animal ectoderm cells. Over-expression of Xfz7 increased the frequency of punctuated F-actin contractions by increasing the stability of the F-actin network. Animal cap ectoderm cells expressing Xfz7 develop dense arrays of actin networks and more contracted network in mid-cell cortex compare to control (Figure 15B). In fact, the rate of punctuated F-actin contractions are increased 4.6 fold in Xfz7 expressing ectoderm cells which also have similar rates of contractions with control mesoderm cells (Figure 15A). Over–expression of Xfz7 in mesoderm cells induced persistent contractions

with a longer life time which might be relate to less elongated cell shapes (LTW 1.51 ± 0.22; 12 cells from 4 explants) than control (LTW 2.11 ± 0.84; 12 cells from 4 explants) (Figure 17; Table 2). FRAP analysis of F-actin within Xfz7 expressing mesoderm cells indicate that contractile, heterogeneous actin network is composed of more stable arrays of F-actin (Figure 15C and D). Thus, expressing exogenous Xfz7 receptors to animal cap ectoderm increases the frequency of actin contractions to levels seen in mesoderm, while increased expression of Xfz7 receptors in mesoderm cells that already have Xfz7 induce more persistent contractions composed of more stable F-actin.

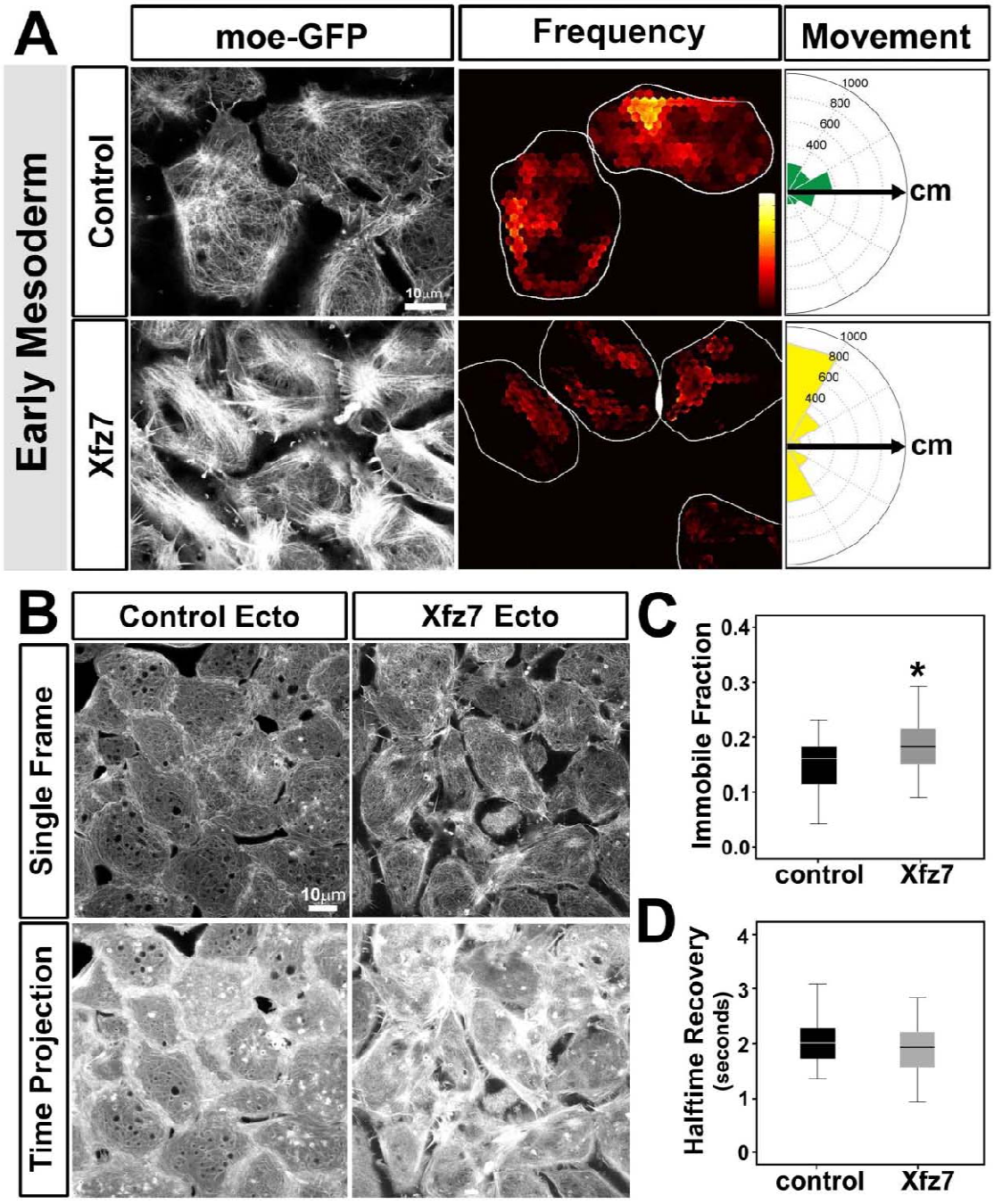

Figure 15. Punctuated actin contractions are modulated by non-canonical Wnt-signaling (I)

(Figure 15. continued) (A) Punctuated F-actin contractions in moe-GFP expressing early mesoderm cells (control and Xfz7 expressing cells) exhibit different patterns of frequency and direction of movement. (cm stands for cell major axis; ** note: direction of punctuated F-actin contractions from round cells like Xfz7 expressing cells (LTW 1.51 ± 0.22); see Supplement Tables) is not considered equally from elongated cells like late mesoderm cells in (Figure 16). (B) Animal cap ectoderm cells expressing moe-GFP (control, Xfz7 expressing cells) and maximum projection of 10 minute time-lapse sequences. (C-D) Xfz7 expressing early mesoderm cells have a significantly high immobile fraction than the control. The heat-map colors in (A) indicate an arbitrary frequency scale from high frequency "light" to low frequency "dark".

Table 2. Quantified dynamics of punctuated F-actin contractions in Xfz7 expressing cells

(Mean ± STD)	Early mesoderm		Animal cap ectoderm	
	control	Xfz7	control	Xfz7
# of explants	4	4	3	3
# of cells	12	12	15	15
Cell shape (LTW)	2.11±0.84	1.51±0.22	1.35±0.25	1.77±0.45
Contractile area (%)	41±13	37±11	18±16	45±10
Rate of contractions (#/hr)	40.5	36.5	8.8	40.8
Life span (min) per Contraction	2.53±2.08	4.40±3.43	2.24±2.05	2.36±2.08
Distance (μm) per Contraction	12.88±12.79	20.78±18	9.56±7.33	12.24±11.46

4.2.2 Altered actin contractions with Xdd1

To test whether down regulation of the non-canonical Wnt-signaling pathway could reduce punctuated contractions we expressed Xdd1 in mesoderm cells. We first confirmed that over-expression of Xdd1 in mesoderm cells can inhibit cell elongation; by late gastrulation Xdd1 expressing mesoderm cells remain round (LTW 1.44 ± 0.24; 15 cells from 5 explants) in the middle of the mesoderm field (prospective notochord) while control mesoderm cells have elongated (LTW 4.13 ± 1.72; 12 cells from 7 explants). Over-expression of Xdd1 blocks the changes in frequency and oriented movements of punctuated F-actin contractions typically seen in dorsal mesoderm (Figure 16A). Mesoderm cells expressing Xdd1 retain similar levels of F-actin as controls both in the mid-cell cortex and lamellipodia, but the frequency of punctuated F-actin contractions is reduced to less than half the frequency of punctuated F-actin contractions than found in control cells (Figure 16A and 17). Furthermore, F-actin contractions in Xdd1 expressing cells move in random directions, whereas the more frequent punctuated F-actin contractions in control cells move parallel to the axis of elongated mesoderm cells (Figure 16A).

To rule out the possibility that Xdd1-overexpression globally alters actin dynamics we expressed moe-GFP and Xdd1 in animal cap ectoderm. Xdd1 has no effect on ectoderm cell shape (Figure 16B). Punctuated F-actin contractions normally found in animal cap ectoderm cells show no distinct patterns in movement. Applying the same image analysis tools we used for the mesoderm, we found no differences between either contractile area, rate of contraction, or direction of movement when we compared F-actin dynamics within control ectoderm cells to Xdd1-expressing ectoderm cells (Figures 16B and 17; see table3).

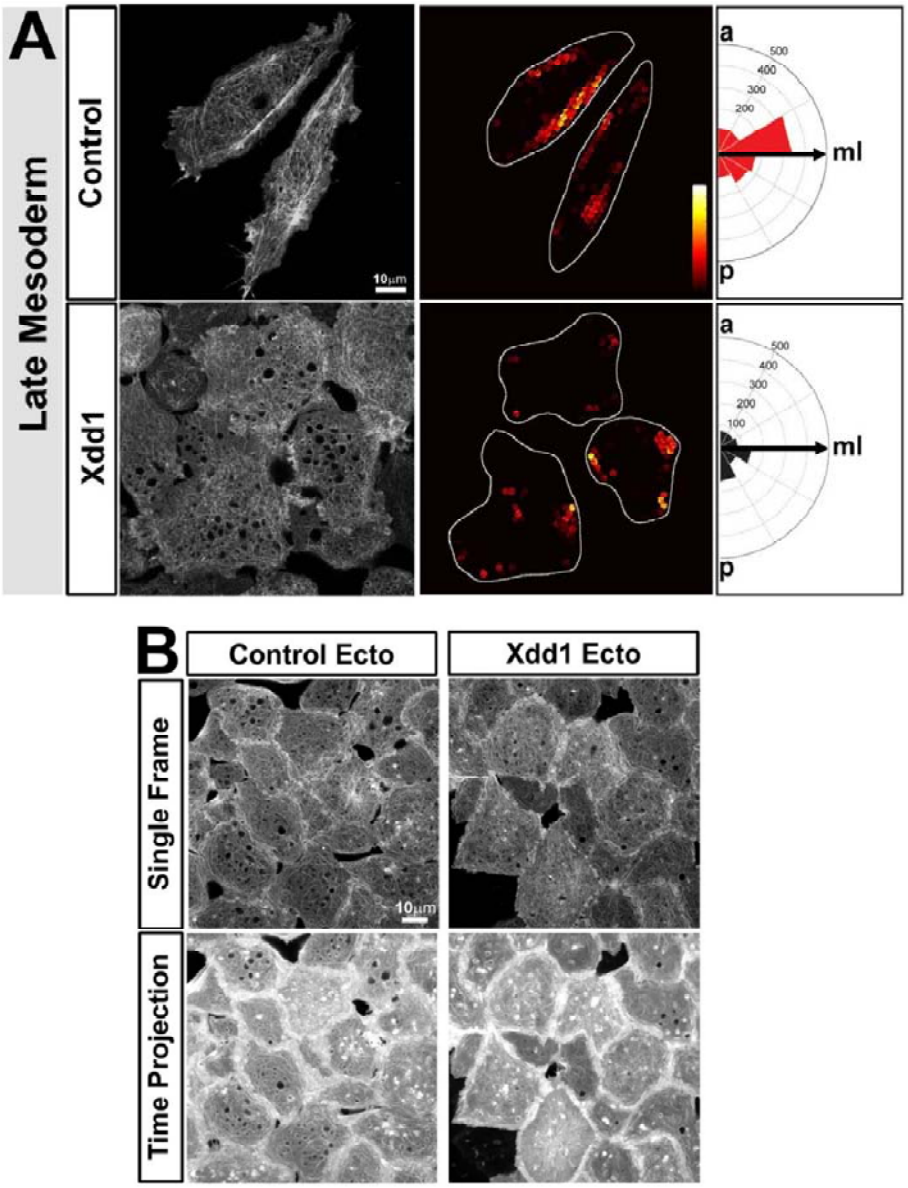

Figure 16. Punctuated actin contractions are modulated by non-canonical Wnt-signaling (II)

(A) Punctuated F-actin contractions in moe-GFP expressing late mesoderm cells (control and Xdd1 expressing cells) exhibit different patterns of frequency and direction of the movements. (ml stands for mediolateral axis) (B) Animal cap ectoderm cells expressing moe-GFP (control and Xdd1 expressing cells) and maximum projection of 10 minute time-lapse sequences. The heat-map colors in (A) indicate an arbitrary frequency scale from high frequency "light" to low frequency "dark".

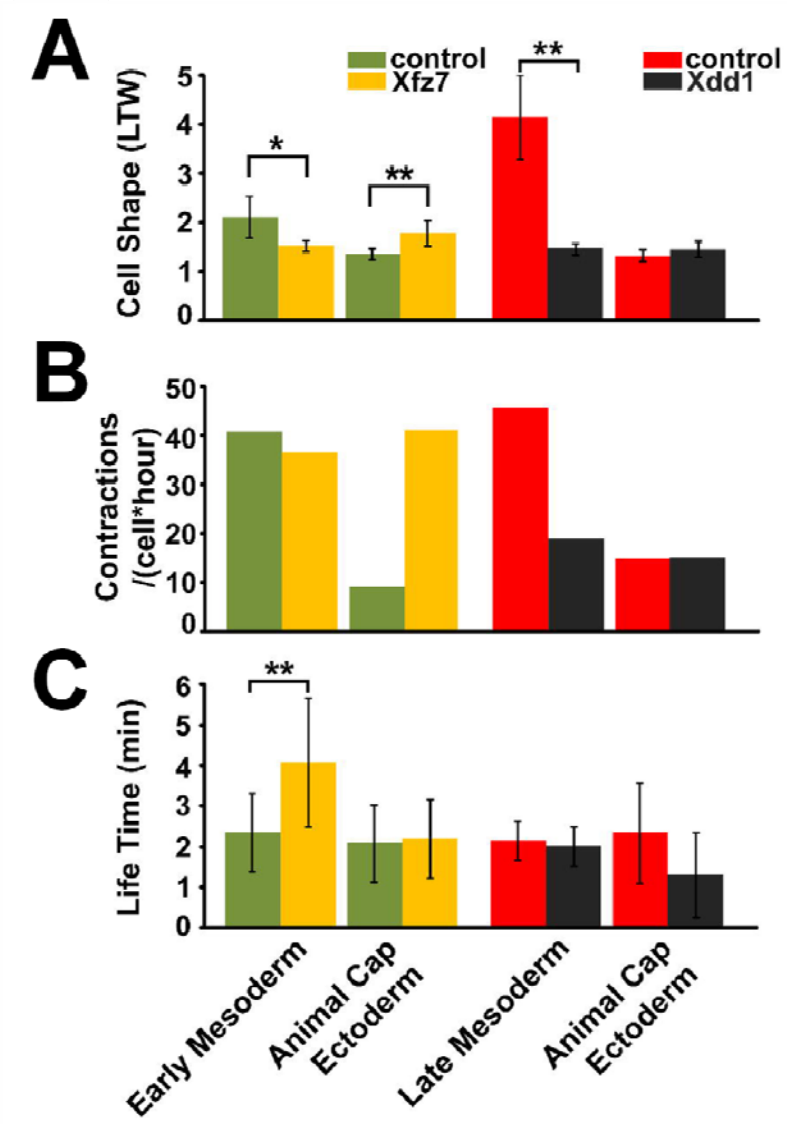

Figure 17. Non-canonical Wnt-signal regulates punctuated actin contractions

(A-C) Quantified results of cell shape, rate and life time of punctuated F-actin contractions from Xfz7 and Xdd1 expressing cells. (* significant differences with $p < 0.05$ level, and ** indicates $p < 0.01$; see table 2 and 3).

Table 3. Quantified dynamics of punctuated F-actin contractions in Xdd1 expressing cells

(Mean ± STD)	Late mesoderm		Animal cap ectoderm	
	control	**Xdd1**	**control**	**Xdd1**
# of explants	7	5	3	6
# of cells	12	15	16	18
Cell shape (LTW)	4.13±1.72	1.44±0.24	1.31±0.24	1.44±0.31
Contractile area (%)	33±11	23±15	14±7	18±23
Rate of contractions (#/hr)	45.5	18.8	14.63	15
Life span (min) per Contraction	2.14±0.95	2±0.97	2.33±2.48	1.29±2.09
Distance (μm) per Contraction	10.51±4.4	8.77±4.45	0.5±0.25	0.35±0.44

4.3 CONCLUSION AND DISCUSSION

While it is widely acknowledged that the non-canonical Wnt-signaling pathway regulates cell behavior the details of that control have not been clear. During gastrulation either too-little or too-much Wnt-signaling inhibit mediolateral elongation and intercalation of mesoderm cells. Furthermore, in some systems Wnt-signaling can proceed in the absence of Wnt-ligands. Our studies suggest that this is due to a permissive role for Wnt-signaling in regulating actomyosin contractility. Xfz7 expressed in embryonic ectoderm can restore mesoderm-levels of actomyosin contractility and can over-stimulate contractions within mesoderm. Xfz7 expressing ectoderm cells with increased rates of punctuated contractions do not elongate or align because they still lack planar polarity cues. Under these conditions Wnt-signaling appears to play a permissive role in regulating cell behaviors through actin contractions. When Wnt-signaling is perturbed in mesoderm both permissive and potentially instructive roles in regulating actin contraction are revealed. Too little signaling reduce actin contractions in mesoderm cells to levels seen Xfz7 expressing ectoderm. Too much signaling enhanced the levels of contractions before mesoderm cells elongate and blocks alignment of contractions with the embryo's mediolateral axis. This later effect could be due to the abrogation of PCP cues or could alternatively abrogate reception of other planar cues that have not yet been identified. Several other sources of planar cues, independent of non-canonical Wnt-signaling pathways, have been implicated in germband elongation (Zallen and Wieschaus 2004) and elongation of the forming oocyte in Drosophila (Frydman and Spradling 2001; Viktorinova, Konig et al. 2009), and may underlie elongation of

Xenopus multicellular aggregates (Green, Dominguez et al. 2004; Ninomiya, Elinson et al. 2004; Ninomiya and Winklbauer 2008).

5.0 MOLECULAR CONTROL OF PUNCTUATED ACTIN CONTRACTIONS

This chapter aims to understand the mechanism for the formation of punctuated F-actin contractions in mesoderm cells.

Most of the contents in this chapter are published in

Kim HY and Davidson LA.,(2011) Punctuated actin contractions during convergent extension and their permissive regulation by the non-canonical Wnt-signaling pathway. Journal of Cell Science; Epub ahead of print.

Zhou J*, **Kim HY***, Wang JH, and Davidson LA., (2010) Macroscopic stiffening of embryonic tissues via microtubules, Rho-GEF, and assembly of contractile bundles of actomyosin. Development .137(16):2785-2794. (*co-first author)

5.1 REGULATION OF PUNCTUATED ACTIN DYNAMICS THROUGH F-ACTIN ASSEMBLY AND MYOSIN CONTRACTILITY

Close visual inspection of a punctuated F-actin contraction over one episode (Figure 8A) indicates that an initially sparse F-actin network evolves into a compact structure which rapidly draws a cortical F-actin network toward a focal point then dissipates the network. This suggests a model where punctuated F-actin contractions form as myosin II motors draw filaments into the contraction and that polymerization increases the density of actin filaments. To separate the role of these two processes in the formation of punctuated F-actin contractions, we used small molecule inhibitors and the protein over-expression that selected to perturb F-actin polymerization and myosin II motor activity separately and assessed the resulting dynamics of F-actin networks in early mesoderm cells before the cells have adopted a strong mediolateral bias to their shape and behavior

To depolymerize or stabilize F-actin, we treated MZ explants with LatB (0.6μM) or, Jasplakinolide (Jas; 5μM) respectively, or over-expressed the Lim Kinase mutant LimK T508EE ($LimK^{CA}$; (Edwards and Gill 1999; Mseka, Bamburg et al. 2007)); to increase or inhibit myosin II induced F-actin contractions, Calyculin A (CalA; a myosin light chain phosphatase inhibitor; 50n M) or Y27632 (a Rho-kinase inhibitor; 50μM) were used. Each inhibitor treatment dramatically changed F-actin networks within 60 to 90 min. Over-expression of $LimK^{CA}$ have been reported previously to phosphorylate Cofilin and increase the assembly of F-actin (Edwards and Gill 1999; Mseka, Bamburg et al. 2007). Mesoderm cells treated with CalA exhibit dense F-actin arrays that move back-and-forth around the cell periphery as well as across the cell cortex. These rapid movements occur in the absence of normal sheet-like lamellipodial protrusions (Figure 18). In contrast, Y27632 did not affect lamellipodial protrusions but resulted in fewer

punctuated F-actin contractions (Figure 18). Cells incubated with Jas showed rapid aggregation of F-actin into a few large focal points within cells. Time-lapse sequences show continuous F-actin flow into these localized sites (Figure 18). Surprisingly, F-actin dynamics in LatB-treated cells share some features with Jas-treated cells. For instance both treatments result in the formation of F-actin aggregates that appear stabilized at specific sites in the cell (Figure 18). The constitutively active LimK induced large star-like F-actin structures with dense F-actin networks (Figure 18). Since single images of F-actin distribution reveal only gross morphology, we processed short duration time-lapse sequences into maximum-intensity projections to highlight regions where repeated F-actin contractions appear as dense persistent networks (Figure 18). High intensities in projected time-lapse sequences reveal more frequent contractions after cells are incubated in either CalA or Jas as well as increased numbers of contractions within $LimK^{CA}$ expressing cells. Low intensity regions in time-lapse projections indicate where contractions are less abundant or less persistent following Y27632 or LatB treatment.

In addition to assessing the morphological changes of actin filaments induced by inhibitors, we monitored the biochemical consequences of these treatments of the actin filaments using fluorescent recovery after photo-bleaching (FRAP;(Axelrod, Koppel et al. 1976; Amato and Taylor 1986)). Fluorescent recovery of moe-GFP was monitored after photo-bleaching a 7 μm by 7 μm region of F-actin cortex within mesoderm cells treated with Jas, Y27632, and CalA, as well as cells expressing $LimK^{CA}$. Cells incubated with Jas show significantly increased immobile fraction as well as increased recovery times (Figure 19A and B) indicating that Jas stabilized F-actin. Similarly, cells expressing $LimK^{CA}$ had stabilized F-actin with significantly increased immobile fraction (Figure 19A).

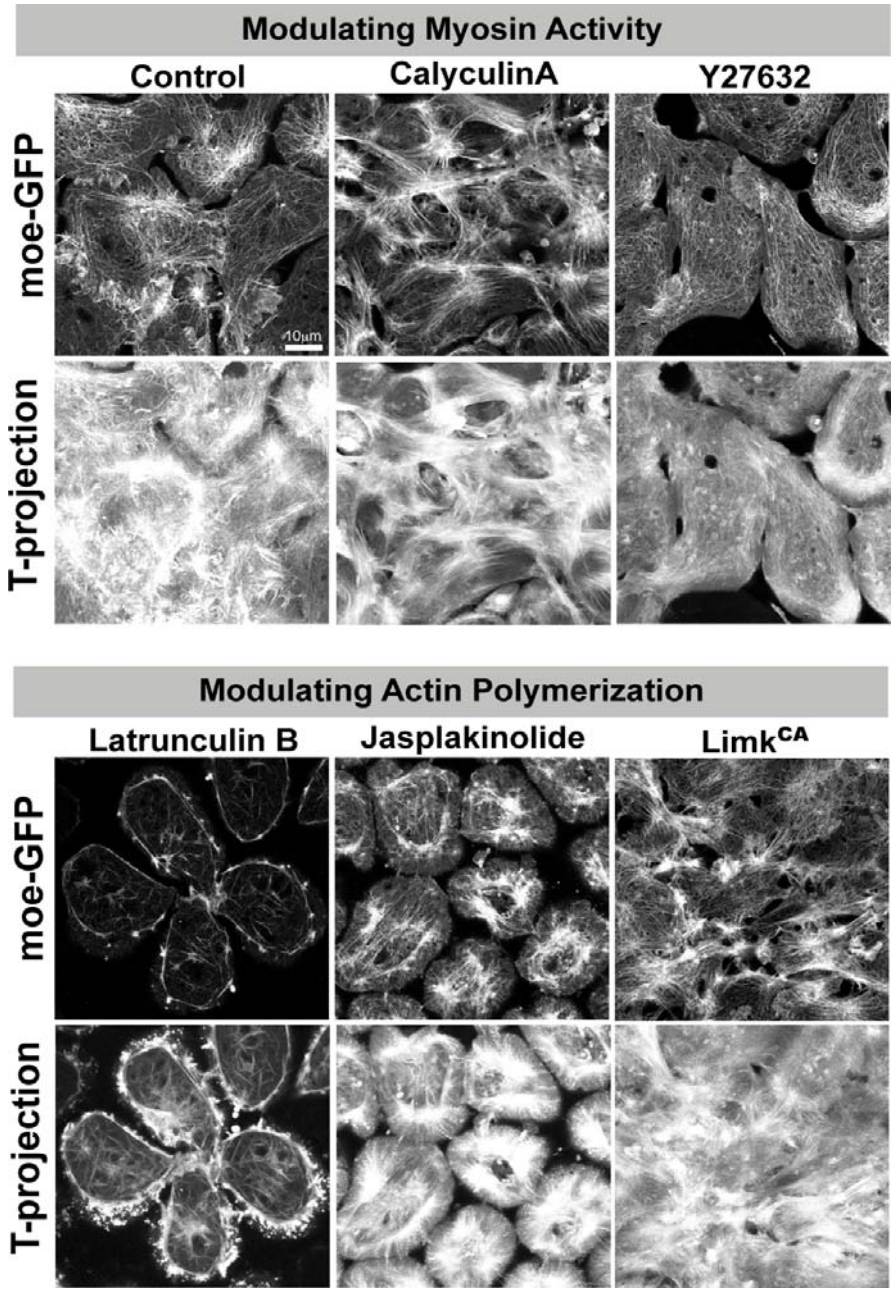

Figure 18. Morphological changes of F-actin induced by inhibitors

Confocal images from representative time-lapse sequence of moe-GFP expressing early mesoderm cells treated with 50nM Calyculin A, 50μM Y27632, 0.6 μM Latrunculin B, 5μM Jasplakinolide and expressed $LimK^{CA}$. The maximum projection of time series of moe-GFP show the overall levels of F-actin dynamics for 10 min during early gastrulation.

Our FRAP data suggests that F-actin aggregates in Jas-treated and $LimK^{CA}$-expressing cells are the result of either enhanced actin polymerization or suppressed the actin depolymerization. $LimK^{CA}$ did not disrupt the F-actin morphology as severely as Jas but our FRAP analysis indicates it has similar effects to Jas on the stability of F-actin. This may be due in part to the unique targeting of LimK and cofilin in embryonic cells, whereas Jasplakinolide may exert global effects on all manners of actin-dependent processes within cells. In contrast, the stability of F-actin in cells treated with inhibitors that modulate myosin activity (Y27632 or CalA) is not altered from controls (Figure 19D), even though these inhibitors produced noticeable changes in the morphology of F-actin (Figure 18).

It is worth noting that there is considerable variation in FRAP results within control cells from the same tissue at the same stage. We wondered whether this variation could be due to heterogeneities in the network morphology, for instance due to differences between contractile and non-contracting regions. To test this we compared FRAP results between these regions and found that increases in the immobile fraction within control group are significantly correlated with the relative initial intensity of the moe-GFP of selected region (Figure 19E; Pearson correlation =0.426; p=0.000). This suggests that punctuated contractions contain a more stable cortex than non-contracting regions. Alternatively, a contractile cortex could affect recovery dynamics by translocating un-bleached F-actin or by recruiting more F-actin into a forming contraction. We also found that F-actin contractions induced by CalA (Figure 19A) exhibited large variance in the immobile fraction. However, regions undergoing punctuated actin contractions did not show altered recovery times (Figure 19F). Due to the technical limits of confocal scanning and the short life-time of F-actin contractions we were not able to resolve differences between the assembly and disassembly phases of punctuated contractions. Thus,

evidence from inhibitor and FRAP studies reveals that punctuated F-actin contractions are the product of coordinated actin polymerization and myosin II activity and that these processes underlie the developmental regulation of the frequency, duration, and movement of contractions within cells.

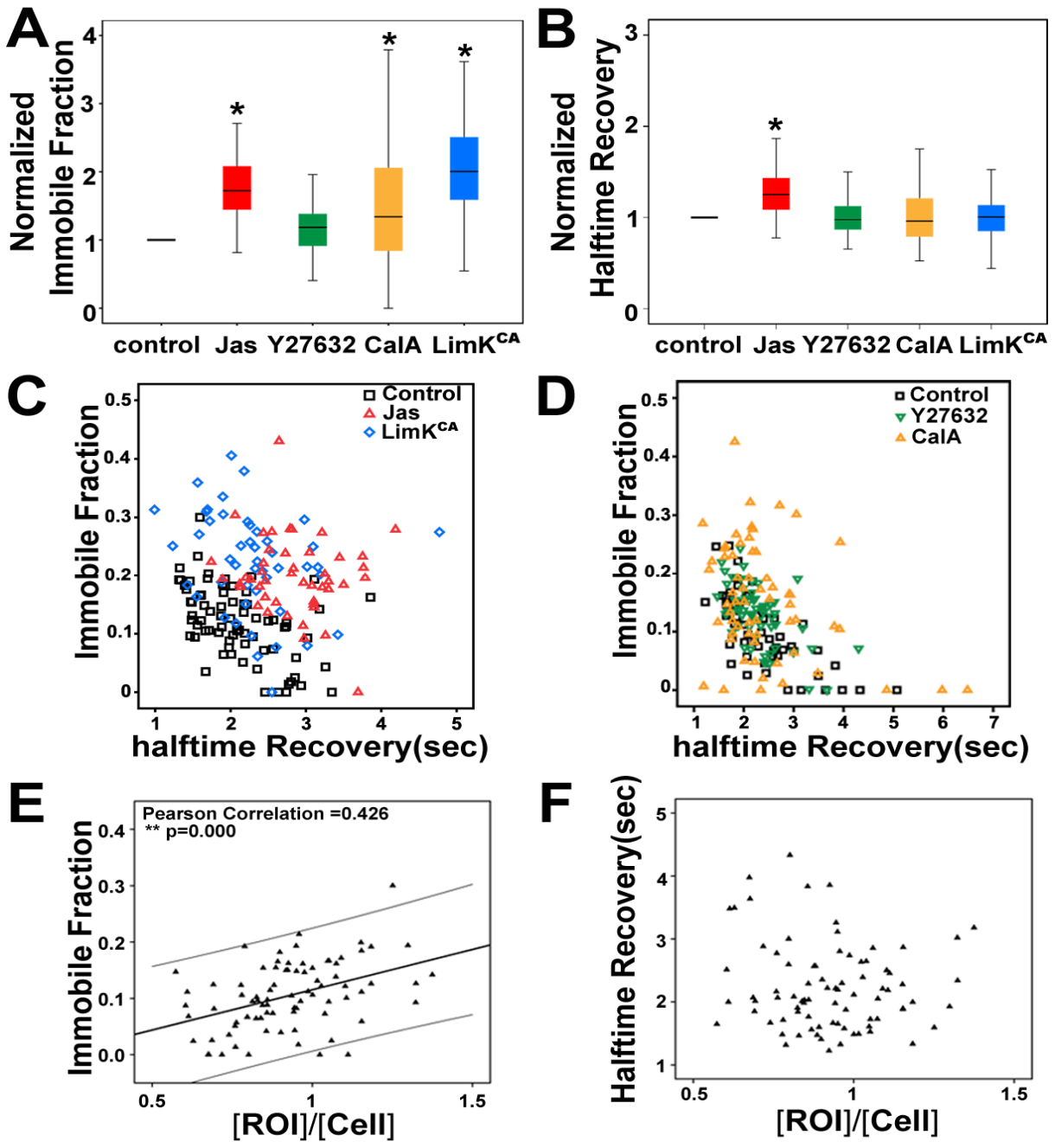

Figure 19. Assessing F-actin dynamics with fluorescent recovery

(A) Immobile fraction (*p < 0.001, 56 control and 46 Jas treated cells) and (B) half time recovery (*p < 0.001, 56 control and 46 Jas treated cells) are significantly higher in Jas treated cells than control cells. (C) Jas treated cells have significantly higher values of the halftime recovery and immobile fraction compare to control cells, (D) although either Y27632 or Cal A treated cells have similar ranges of both

immobile fraction and half time recovery compare to control ones. (E) The brighter cortex has higher immobile fraction after photo bleaching within control cells. X axis represents the ratio of moe-GFP intensity of bleached region to the intensity over the entire cell prior to photo-bleaching. For control cells, pre-bleach intensity levels of bleached area are positively correlated with immobile fraction (person correlation =0.426 (a slope with 95% confidence interval), ** $p < 0.001$, 82 control cells), but (F) no correlation with half time recovery.

5.2 REGULATION OF PUNCTUATED ACTIN DYNAMICS THROUGH MICROTUBULE BINDING RHOGEF

In addition to actin cytoskeleton, microtubule is considered to be a major cytoskeletal component that involved in diverse cellular functions such as cell migration and cell adhesion, and accounted as structural elements in regulating cell stiffness and force production (Kaverina, Krylyshkina et al. 1999; Small and Kaverina 2003). Now evidences are accumulating that cytoskeletal elements participate in regulating each other and their coordination is achieved through common regulator like RhoGTPases. For instance, microtubules can signal to actomyosin through Rho family GTPases. RhoGTPases are key elements in the regulation of the actomyosin cytoskeleton in both cultured cells and during morphogenesis (Hall 2005). The Rho family members are well known to control cellular processes such as actin assembly as well as the organization of myosin II mediated contractility into lamellipodia and filopodia to guide cell migration and cell contractility.

The model for microtubule binding RhoGEF, RhoGEF-H1, function proposed by Bokoch and coworkers (Birkenfeld, Nalbant et al. 2008; Chang, Nalbant et al. 2008) suggests that when bound to microtubules RhoGEF H1 is inactive; however, once released from microtubules RhoGEF H1 activates RhoA (Chang, Nalbant et al. 2008). In addition, the *Xenopus* homolog of GEF-H1 (XLfc, after mouse homolog GEF-HI,Lfc) has been already cloned (Morgan, Hooiveld et al. 1999) and reported the co localization with microtubule (Kwan and Kirschner 2005).

Based on the model the microtubule binding RhoGEF, Xlfc, can activate RhoA, we want to induce both actin assembly and myosin contractility with the activated Rho that associated with dynamics of microtubule assembly. To control the polymerization dynamics of microtubules nocodazole (50μM; depolymerize MT) was used. To confirm that nocodazole reduced the density of microtubules we visualized microtubules in living *Xenopus* explants using high resolution confocal time-lapse microscopy of explants expressing tau-GFP (Figure 20; (Kwan and Kirschner 2005)). High doses of nocodazole did not completely inhibit microtubules but reduced them in agreement with previous studies (Lane and Keller 1997; Kwan and Kirschner 2005). We monitored the changes of F-actin with the same treatments by visualizing live F-actin with expressing mRNA encoding moe-GFP. In about 70 minutes of nocodazole treatment we found dense F-actin bundles assembled and contract the cell that force to shape round within a tissue (Figure 20).

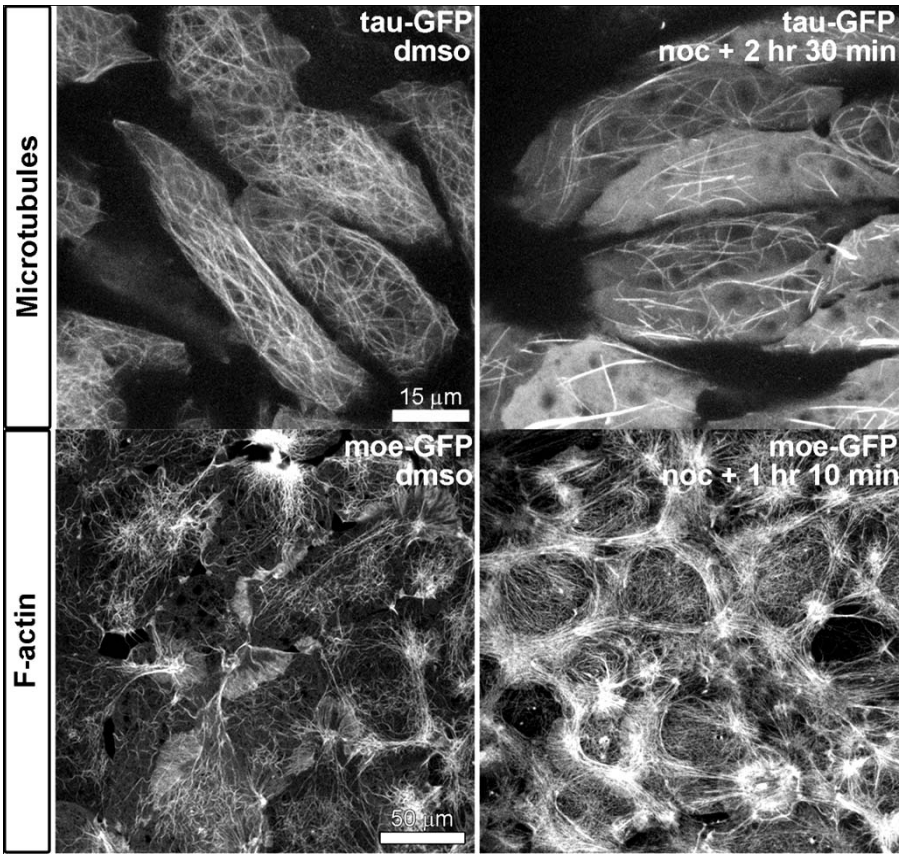

Figure 20. Depolymerized Microtubule induces F-actin Assembly

Tau-GFP expressed in mesodermal cells in marginal zone explants reports the presence of microtubules and that nocodazole reduces the amount of microtubules. Moe-GFP expressed in mesodermal cells in marginal zone explants reports the presence of F-actin and that nocodazole-treatment leads to increased amounts of F-actin over the same time-scale.

To confirm the effect of XLfc released from MT to activate actomyosin contraction, we knockdown XLfc then induce the MT depolymerization with nocodazole, then check changes of F-acitn. To inhibit the MT mediating XLfc effect, we knockdown the XLfc by injecting antisense morpholino of XLfc (XLfc-MO) and have the control set by using the control morpholino (XLfc- CO). Embryos expressing half of XLfc-MO treated with nocodazole clearly show the induced F-actin bundling on the XLfc-MO uninjected side, but no changes in MO injected side (Figure 21B and E-E'). There are no differences in F-actin in XLfc-CO injected sides, and respond to the nocodazole treatment like no-injection control (Figure 21).

Thus we confirmed that Xlfc-MO reduced the level of nocodazole-induced F-actin assembly in *Xenopus* explants. We then confirmed that the inducing F-actin assembly activity of nocodazole-released Xlfc could be recapitulated by the point-mutant Xlfc C55R, a constitutively active GEF (Kwan and Kirschner 2005). Whole embryos expressing Xlfc C55R at high doses showed severe defects similar to those seen after over-expression of activated RhoGTPase (Tahinci and Symes 2003)(data not shown). Reliable tissue explants could not be prepared from these embryos so we lowered the amount of Xlfc C55R mRNA injected to 175pg per embryo, allowing majority of embryos to gastrulate successfully. Tissues isolated from these embryos showed sharp increases in F-actin in explants expressing moe-GFP (Figure 21C). Thus, the RhoGEF activity of Xlfc is both necessary and sufficient to enrich F-actin in dorsal explants.

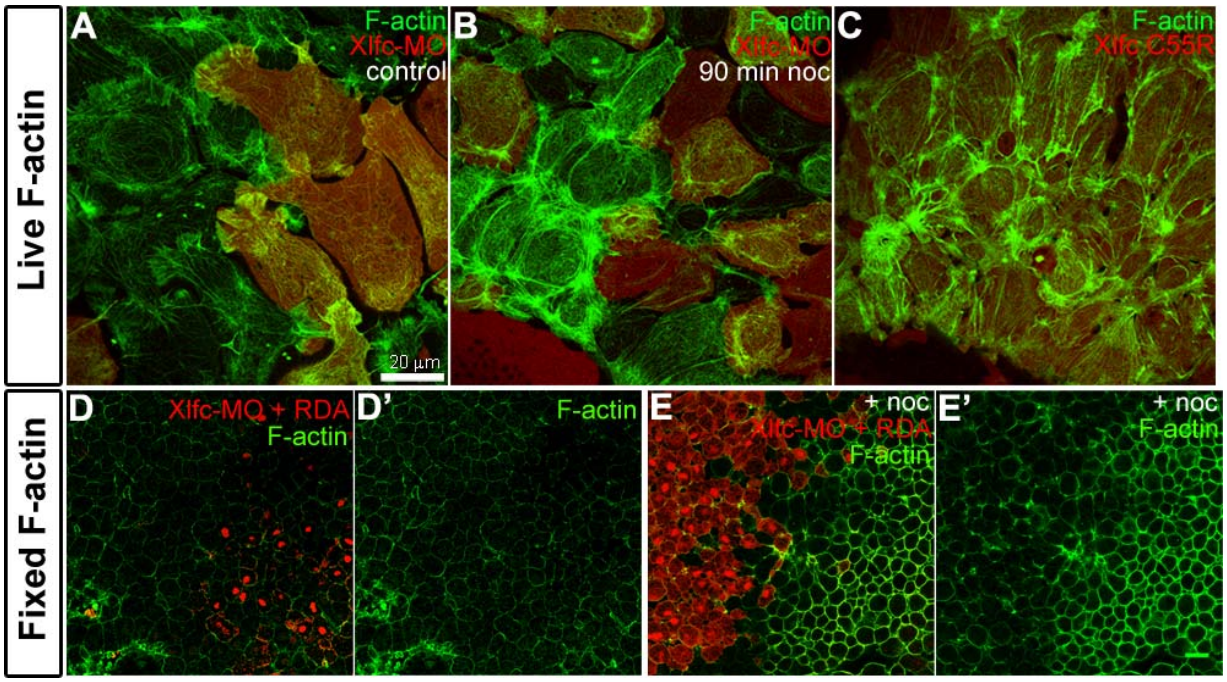

Figure 21. Microtubule binding RhoGEF mediates F-actin Assembly

(A) Moe-GFP expressed in all cells but Xlfc-MO and rhodamine dextran (red cells) co-injected into single animal blastomeres at the 4- to 8-cell stage show no difference in F-actin (green) localization or density in control treated cells in marginal zone explants. (B) Xlfc-MO inhibits excess assembly of F-actin that occurs after 90 minute incubation in 50 µM nocodazole. (C) Xlfc C55R coinjected with moe-GFP and rhodamine dextran induces F-actin assembly to a similar degree to that induced by nocodazole-treatment. (D) Embryos injected in 1 blastomere at 4-cell stage with Xlfc-MO and rhodamine dextran show no changes in endogenous F-actin levels. (E) Endogenous F-actin levels increase in the uninjected side once embryos are incubated with 50 µM nocodazole. (D' and E' show levels of F-actin without RDA-labeled channels of D and E, respectively.)

5.2.1 Induced actin contractions increase cell tractions

Danowski (1989) observed single fibroblasts became much more contractile after treatment with nocodazole and we wondered whether nocodazole-treated *Xenopus* cells within tissues behaved similarly. In order to determine whether *Xenopus* cells incubated in nocodazole exhibited similar increased forces of contractility we turned to culturing tissue explants on force reporting polyacrylamide gels. Small fluorescent beads were co-polymerized with the gel to allow detection of small deformations within the gel. Marginal zone explants isolated from early gastrula stage embryos expressing a membrane-targeted GFP were cultured on the gel (Figure 22A) with elastic modulus of ~1000 Pa for 1 hour before either DMSO or 50 μM nocodazole was added to the media. Cell behaviors and bead movements were tracked using confocal time-lapse microscopy (Figure 22B). One hour later, membrane targeted GFP (Figure 22C) and red-fluorescent microsphere beads (Figure 22D) at the surface of the gel (Figure 22D) were followed in single confocal sections collected at 60 second intervals.

Resolving traction under *Xenopus* explants undergoing morphogenesis required development of a novel approach. Conventional approaches to measuring traction forces generated by cultured cells or small numbers of *Xenopus* embryonic cells involve identification and tracking of individual beads and the removal of the cell or tissue at the conclusion of the experiment to obtain bead positions for the "zero-force" state (Beningo, Lo et al. 2002; Dzamba, Jakab et al. 2009; Trepat, Wasserman et al. 2009). Comparing "zero-force" bead positions with the positions of beads under live explants is made very difficult due to morphogenetic movements within cultured *Xenopus* explants. Coordinated cell movements in *Xenopus* explants can take several hours after tissues are microsurgically removed before they are reliable. During that time, tissue movements begin to reshape the explant (Davidson, Keller et al. 2004) and

generate both microscopic forces under cells and macroscopic forces both in and out of the plane of the explant (Zhou et al, in prep). Removing *Xenopus* tissues not only releases cells from the substrate but also releases the macroscopic forces throughout the explant. Thus, to measure traction forces we turned to developing a method that would allow us to identify temporal changes in traction.

Temporal changes in traction are more relevant to the dynamic microenvironment of intercalating mesodermal cells. *Xenopus* embryonic cells move and extend protrusions in a punctuated manner. Preliminary analyses of beads showed that they too undergo punctuated cycles of movement interspersed with quiescent periods. To analyze temporal changes in traction over an entire field of cells we developed a quantitative method based on image registration (Arganda-Carreras, Sorzano et al. 2006) for measuring the absolute displacements of the gel.

This method allows visualization of displacements to be combined with confocal sections collected from explants expressing mem-GFP. To validate this method we assessed the algorithm used to measure traction under nocodazole-treated explants in null-force conditions, with two random bead images, and after point forces have been applied to the surface of a gel by a mechanical probe (see Appendix A). Thus, the image registration method allows us to compare temporal patterns of traction generated within an entire field of cells.

Traction generated by a field of mediolaterally intercalating mesodermal cells in marginal zone explants was quantified using the image registration method. Image registration produces a pixel-by-pixel map of cell tractions based on the direction and magnitude of movements in the gel substrate beneath multicellular tissues. From this map we can visualize the degree of substrate movement beneath intercalating cells and using histograms we can quantify areas of high contraction. DMSO-treated control explants containing elongating mesodermal cells

generated heterogeneous patterns of traction over 20 minutes (Figure 22E). However, identically staged elongating mesoderm cells in nocodazole-treated explants generate greater traction over a much larger area (Figure 22F). To quantify the changes in high-traction areas we compared histograms of traction maps from DMSO controls their matching nocodazole-treated traction maps. Traction maps from control explants show 10% of the map exhibit displacements greater than 0.34 μm. In contrast, more than 67% of the traction map shows traction greater than 0.34 μm-displacements. Thus, nocodazole causes high traction areas to increase from 10% to 67% or a 6.7-fold increase. Similar analysis reveals areas covered by the highest levels of traction expand to 53% (set 2) and 77% (set 3) of the total area under the explants. Thus the areas with the highest 10% of tractions are expanded in area 6.7-, 5.3-, and 7.7- fold.

Traction maps combined with confocal images of cell shape reveal that traction mediated bead displacement is highest at sites of cell-cell junctions localized at the mediolateral ends of intercalating cells (arrowheads; Figure 22G and H). Analysis of mesodermal cells in explants from three different clutches of embryos reveals some differences in base levels of traction (Figure 22I) but all cases show that nocodazole induces substantially higher mean traction than control explants (Figure 22J). Thus, nocodazole treatment activates Xlfc RhoGEF, increases actomyosin contractility and bundling, and induces cell traction or contractility.

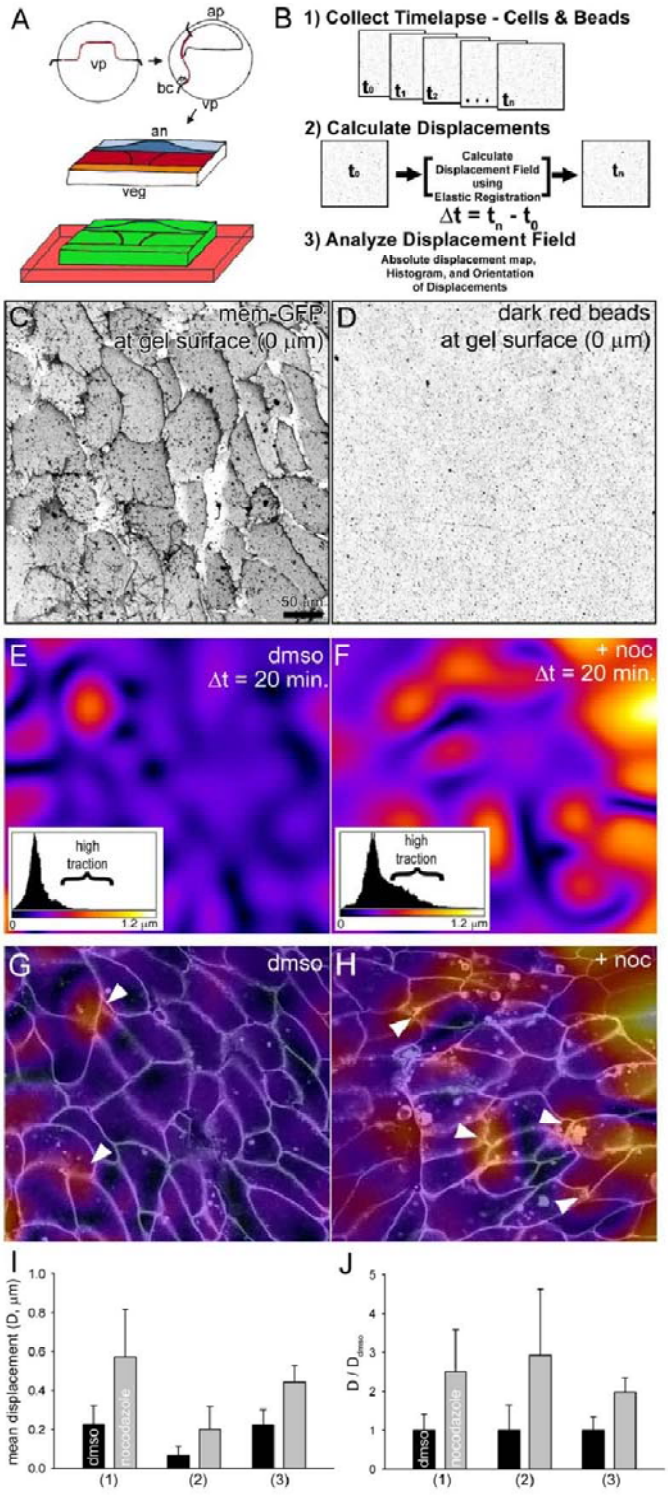

Figure 22. Traction maps reveal nocodazole increases contractility of tissue

(Figure 22. continued)

(A) Assembly of marginal zone explants on displacement-reporting polyacrylamide gels. (B) Traction maps are calculated from confocal time-lapse sequences of gel, cell, and tissue movements. (C) Confocal section of mesodermal cells expressing a membrane localizing GFP (mem-GFP) cultured on fibronectin-conjugated polyacrylamide gel. (D) Confocal section collected at the same level shows the position of dark red fluorescent microsphere beads on the surface of the gel. (E) Traction map shows the magnitude of bead displacements beneath mesodermal cells within an intact marginal zone explant incubated in DMSO. The inset histogram shows the frequency of bead displacements and the scale of displacements. Most displacements are limited to less than 0.3 μm within the color-range of purple to blue; regions of high traction above 0.3 μm are within the color-ranges of red to yellow. (F) Traction map of mesodermal cells in explants incubated in 50 μM nocodazole show large displacements spread over larger areas. The histogram shows a large increase in regions of high traction. (G and H) Combine displacement maps shown in E and F, respectively, with overlying cell outlines collected from a confocal section 5 μm deeper into the cells. High regions of traction in both DMSO and after incubation in nocodazole appear to co-localize with cell-cell junctions at the mediolateral ends of cells (arrowheads). (I) Mean displacements calculated from the full field of view collected from three explants from three clutches show significant and large increases in traction after explants are incubated in nocodazole. Variances from clutch to clutch may reflect slight changes in substrate preparation or clutch-to-clutch differences in cell-generated traction. (J) Mean displacements normalized for each clutch show nocodazole consistently increases traction in all cases.

5.3 CONCLUSION AND DISCUSSION

Our description of punctuated actin contractions, observations of both F-actin morphology and changes in dynamics following inhibition of actin polymerization or myosin II contractility suggest a complex model for punctuated contractions. Such a model requires spatially constrained and rapid regulation of myosin function as well as control over the assembly and disassembly of F-actin. In the first few seconds of a contraction we observe F-actin moving toward the future center of the contraction. This suggests the first step involves modulation of myosin light chain activity within a small region of the sparse F-actin cortex. However, this slight movement of F-actin toward a focus does not appear to be sufficient to account for the rapid increase in F-actin as the contraction reaches its peak. To account for this increase and the results of our FRAP experiments we propose a rapid increase in both polymerization and depolymerization of F-actin. The net effect of this "churning" is to increase the abundance of F-actin within a contraction but does not change its life-time. As the contraction dissipates the rates of depolymerization must offset polymerization. The observation that F-actin is nearly absent after myosin II knock-down (Skoglund, Rolo et al. 2008) is surprising but this may reflect feedback mechanisms that adjust mechanical resistance to match available force-generation (Davidson, von Dassow et al. 2009).

In addition to the contributions of actin assembly and myosin contractility to the formation of punctuated actin contractions, we found that RhoGEFs released from microtubule depolymerization mediate activation of actomyosin contractility. Nocodazole, microtubule depolymerizing drug, effects on the activation cell contractility by RhoGEF-H1 and are blocked by morpholinos that knock-down synthesis of the *Xenopus* homolog Xlfc. Furthermore, the induced actomyosin contractility via RhoGEFs increases cell tractions within *Xenopus* tissue and

indicate regulation of cortical actin contractions through microtubule assembly. Parallel studies in our lab demonstrate that microtubule depolymerization increases dorsal tissue stiffness in *Xenopus* through the activation of actomyosin contractility results in developmental defects (Zhou, Kim et al. 2010). These results extend earlier observations that microtubules repress single cultured cell contractility and that cell contractility can regulate embryonic tissue stiffness. These same reagents have been previously used to investigate the role of Xlfc and nocodazole in controlling polarized cell behaviors during convergent extension (Kwan and Kirschner 2005) and we have shown that they also alter the mechanical microenvironment and globally increase levels of cell contractility. In light of our findings, we suggest a re-evaluation of the role of microtubules in regulating both cell behaviors and the mechanics of morphogenetic movements because of the prevalent use of microtubule depolymerizing drugs such as nocodazole.

6.0 CONCLUSION

6.1 SUMMARY

We aim to understand the role of dynamic actin cytoskeleton that underlies cell behaviors during convergence and extension in developing frog embryo. The aims are framed to examine the dynamics of cortical F-actin within cells in converging and extending tissue, to understand the regulation of the actin dynamics through non-canonical Wnt-signaling, and through molecules involved in assembly of the actomyosin contractions.

We used moe-GFP to label live F-actin and found rapidly moving F-actin features that cycle through assembled F-actin contraction followed by dissipation, referred as punctuated F-actin contractions. We designed image analysis tool to quantify the spatial and temporal frequency and moving distances and orientations of punctuated actin dynamics that can be used to contrast the actin dynamics among cells in different conditions. Interestingly, the punctuated F-actin contraction which is closely related to cell behaviors have distinct pattern across the dorsal marginal zone explants transition. The punctuated actin contractions moves in directions from random to orient to elongated axis as mesoderm cells undergo mediolateral cell intercalation during convergence and extension. In order to understand the mechanism that regulates the oriented movements of punctuated actin contractions, we chose to investigate the role of the non-canonical Wnt-signaling pathway that is known to send signals which polarize

mesoderm cells, in addition to reorganize the actin cytoskeleton. Increasing the non-canonical Wnt-signals by Xfz7 in ectoderm was sufficient to induce high actin contractions seen in mesoderm. Blocking the signals in mesoderm with Xdd1 reduced the frequency and blocked the oriented movements of punctuated F-actin contractions. These results from Xfz7 and Xdd1 expression indicate the punctuated actin contractions are under permissive regulation of non-canonical Wnt-signals.

The punctuated F-actin contraction seems to be assembled through F-actin polymerization and myosin contractility. Results from using small molecular inhibitors that separately alter the dynamics of F-actin and myosin combined with monitoring changes in F-actin morphology and the recovery of moe-GFP after photo-bleaching suggest the essential role of myosin contractility for forming the punctuated actin contraction.

We also found that RhoGEFs released from microtubule, Xlfc, activate the cortical actin contractions, and strongly induced actin bundling and contractions. The increased cell tractions via Xlfc result in increasing tissue stiffening 2- to 3-fold (Zhou, Kim et al. 2010) and lead to defects in morphogenesis. Our findings suggest a role of microtubule in establishing mechanical properties of cells and tissues, and re-evaluation of the role of microtubules in morphogenesis. We suspect the disruption of several morphogenetic movements from use of nocodazole such as failure of blastopore closure in frog (Lane and Keller 1997), epiboly in zebrafish (Solnica-Krezel and Driever 1994) and the epithelial to mesenchymal transition in chick gastrulation (Nakaya, Sukowati et al. 2008) may be due to elevated levels of actomyosin contraction or global stiffening of embryonic tissues. These findings complement the mechanical studies and provide a link between subcellular dynamics and macroscopic behaviors of tissues.

6.2 FUTURE DIRECTIONS

The punctuated F-actin contractions are a shared dynamic of actomyosin network within cells in developing *Xenopus* embryos, yet show distinct patterns of frequency, localization, and movements among different cell types. We may consider a single episode of punctuated F-actin contractions and a lamellipodia protrusion as parallel F-actin machineries that can help to drive cell shape changes. For instance, F-actin mesh under the plasma membrane undergo continuous contraction and relaxation cycles which can integrate to change cell shape for punctuated acin contractions, and directed actin polymerization within lamellipodia protrusions can also lead the cell shape changes.

However, there are many questions to address in order to understand the mechanisms that control punctuated actin contractions. For example, understanding how physical and chemical signals direct the contractions, details about molecular control of formation of contractions, and feedback mechanism to organize the punctuated contractions within the embryos.

In the current study, we have observed dramatic morphological changes of F-actin with acute inhibitors; however the complex output lead the least conclusion for the contraction where both actin polymerization and myosin contractility are responsible for assembly of the punctuated F-actin contraction. To dissect this complex molecular control, further studies are required, such as a computer simulation of the model that represents the punctuated actin contractions with simple factors like filaments and motor proteins. This simulation approach could recapitulate the contractions *in vivo* and could suggest detailed assembly dynamics which are technically difficult to follow in live cells on the molecular level.

Furthermore, studies are required to investigate the mechanical interactions between neighboring cells or extracellular matrix and the cortical actin contractions which are closely related cell movements, tractions, and tissue stiffness. Our previous findings indicate the importance of the mechanics of morphogenesis through induced actomyosin contractions results in increasing tissue stiffness and the failure of morphogenesis (Zhou, Kim et al. 2009). Additionally we showed increased level of tractions after nocodazole treatments mediate tissue stiffening.

The increased traction can be from both cell contraction (i.e. internal force generation) and adhesion to gel-bound fibronectin. For example, increased tractions could be achieved by increasing the number of focal adhesions or the force produced at each adhesion or some combination of the two. Our current studies with traction-reporting gels do not distinguish between these mechanisms. To resolve the relative contribution of cell adhesion to cell traction, future studies will be needed to identify discrete sites of cell adhesion, the direction and magnitude of force generation at these sites, and how efficiently cells within a tissue transmit intracellular forces to extracellular matrix or gel substrates. We suspect the disruption of morphogenetic movements may be due to elevated levels of actomyosin contraction or global stiffening of embryonic tissues. High levels of contractility may alter cell shapes, causing cells to shorten and round. Altered levels of cell surface contractility may also alter the capacity of cells to rearrange themselves (Puech, Taubenberger et al. 2005) or their ability to maintain tissue polarity (Ninomiya and Winklbauer 2008). Global stiffening may result in tissues ‘locking-up’ or becoming too stiff for normal levels of force generation to bend or fold tissues. It is clear that the roles of microtubules are diverse in cells and during development, but future efforts will need a

broader focus on the integrative mechanics and the contribution of different molecular, cellular and tissue-scale structures to the movements of morphogenesis.

APPENDIX A

A1. VALIDATING THE IMAGE REGISTRATION METHOD

To validate the image registration method for determining gel displacement, we take four approaches (Figure 23). Nocodazole induces increased displacements in the adhesive gel substrates beneath mesodermal cells in marginal zone explants (Figure 23A). Registration was carried out using the setting "VeryFine". This setting uses 16 β-spline functions to register displacements along each axis. This is analogous to resolving the displacement of 32x32 pixel subdomains within the 512 x 512 pixel image pairs. The scale displacements in control explants and after nocodazole treatment may vary but larger displacements are seen over larger regions. To determine effect of the number of β-spline used during registration we analyzed displacements between nocodazole-treated image pairs (in A) using the "Fine" (8 β-spline functions in each axis) and "SuperFine" (32 β-spline functions) settings in BUnwarpJ (Arganda-Carreras, Sorzano et al. 2006)(Figure 23B). The overall pattern and histograms of displacements reveals little qualitative differences between these two settings. However, higher maximum displacements are seen after 32 β-splines are used due to the "smoothing" effect seen when fewer β-splines are used. We have used the "Very Fine" settings for all analyses presented here. To determine the background error induced by "jitter" in collecting confocal time-lapse sequences

we collected time-lapse sequences of gel with no explants attached (Figure 23C). Small displacements are detected but few large traction sites are visible. The image registration method seeks to find the "best-fit" displacement that brings on image into registration with another. Artifactual displacements can be produced when trying to map displacements between un-related images (Figure 23D). We created a displacement map between two different images of bead fields. Large artifactual displacements up to 7μm are needed to align these unrelated images. (Note: the scale for this image differs from those in A, B, and C.) To validate that image registration could identify small, localized forces, we used a fine glass needle to apply a displacement to the surface of a traction-reporting gel (Figure 23E and F). The contact region produces a 0.5μm displacement against a background of showing less than 0.1μm displacements. The field of view is 97 μm across.

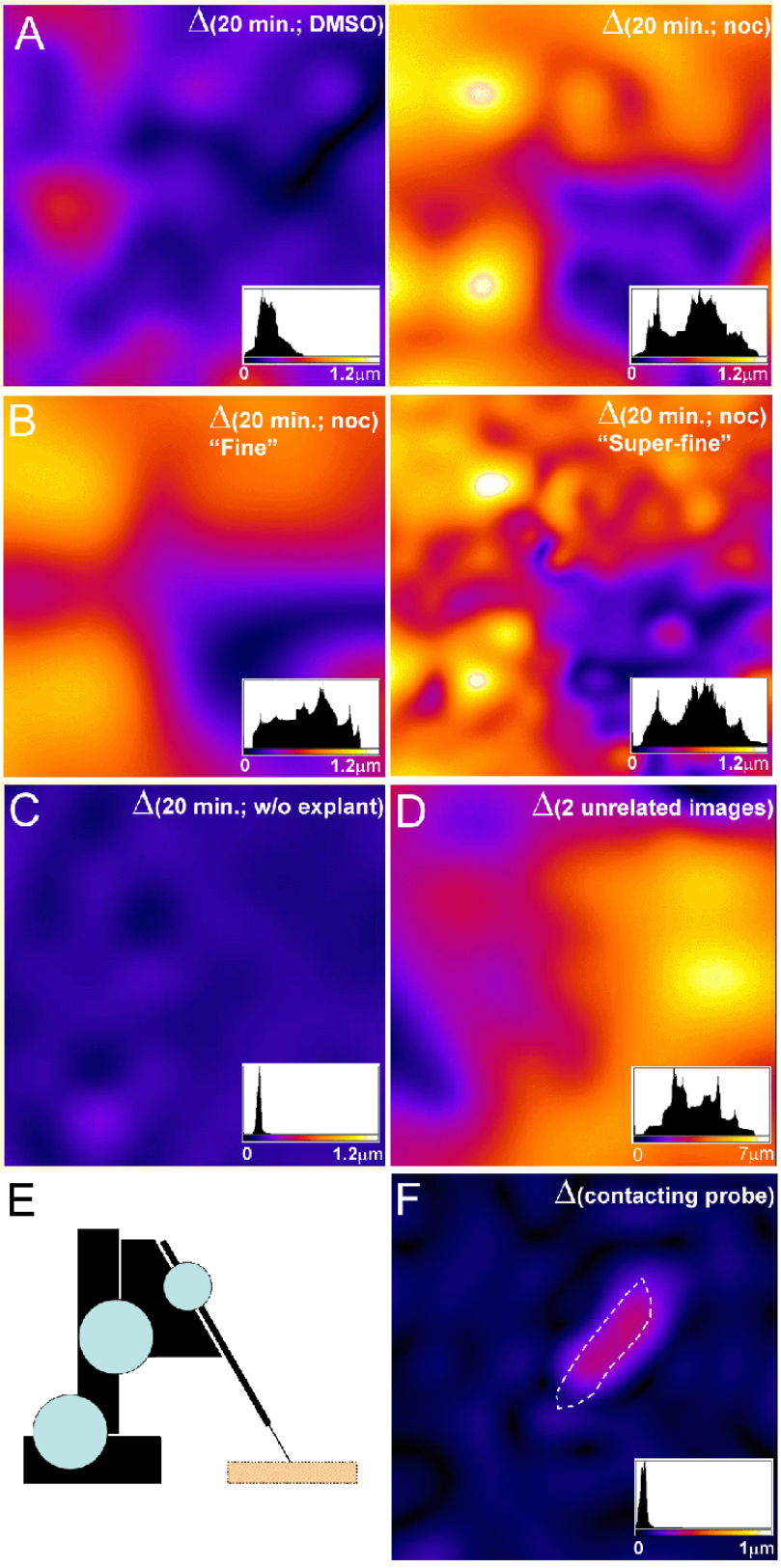

Figure 23. Validating the image registration method

BIBLIOGRAPHY

Amato, P. A. and D. L. Taylor (1986). "Probing the mechanism of incorporation of fluorescently labeled actin into stress fibers." J Cell Biol **102**(3): 1074-84.

Amonlirdviman, K., N. A. Khare, et al. (2005). "Mathematical Modeling of Planar Cell Polarity to Understand Domineering Nonautonomy." Science **307**(5708): 423-426.

Anderson, D. C., J. S. Gill, et al. (2008). "Polarization of the C. elegans Embryo by RhoGAP-Mediated Exclusion of PAR-6 from Cell Contacts." Science **320**(5884): 1771-1774.

Arganda-Carreras, I., C. O. S. Sorzano, et al. (2006). "Consistent and elastic registration of histological sections using vector-spline regularization." CVAMIA:Computer Vision Approaches to Medical Image Analysis: **4241**: 85-95.

Axelrod, D., D. E. Koppel, et al. (1976). "Mobility measurement by analysis of fluorescence photobleaching recovery kinetics." Biophys J **16**(9): 1055-69.

Beningo, K. A., C. M. Lo, et al. (2002). "Flexible polyacrylamide substrata for the analysis of mechanical interactions at cell-substratum adhesions." Methods Cell Biol **69**: 325-39.

Birkenfeld, J., P. Nalbant, et al. (2008). "Cellular functions of GEF-H1, a microtubule-regulated Rho-GEF: is altered GEF-H1 activity a crucial determinant of disease pathogenesis?" Trends in Cell Biology **18**(5): 210-219.

Blalock, H. M. (1972). *Social statistics*. New York, McGraw-Hill.

Blanchard, G. B., S. Murugesu, et al. (2010). "Cytoskeletal dynamics and supracellular organisation of cell shape fluctuations during dorsal closure." Development **137**(16): 2743-52.

Box, G. E. P., and G. M. Jenkins (1976). *Time series analysis: Forecasting and control*. San Francisco: Holden-Day.

Bray, D. and J. G. White (1988). "Cortical flow in animal cells." Science **239**(4842): 883-888.

Brian M. Burkel, G. v. D. W. M. B. (2007). "Versatile fluorescent probes for actin filaments based on the actin-binding domain of utrophin." Cell Motility and the Cytoskeleton **64**(11): 822-832.

Carmona-Fontaine, C., H. K. Matthews, et al. (2008). "Contact inhibition of locomotion in vivo controls neural crest directional migration." Nature **456**(7224): 957-961.

Chang, Y.-C., P. Nalbant, et al. (2008). "GEF-H1 Couples Nocodazole-induced Microtubule Disassembly to Cell Contractility via RhoA." Mol. Biol. Cell **19**(5): 2147-2153.

Charras, G. T. (2008). "A short history of blebbing." J Microsc **231**(3): 466-78.

Copp, A. J., N. D. E. Greene, et al. (2003). "The genetic basis of mammalian neurulation." Nat Rev Genet **4**(10): 784-793.

Cowan, C. R. and A. A. Hyman (2007). "Acto-myosin reorganization and PAR polarity in C. elegans." Development **134**(6): 1035-1043.

Danowski, B. A. (1989). "Fibroblast contractility and actin organization are stimulated by microtubule inhibitors." Journal of Cell Science **93 (Pt 2)**: 255-66.

Davidson, L., M. von Dassow, et al. (2009). "Multi-scale mechanics from molecules to morphogenesis." Int J Biochem Cell Biol **41**: 2147-62.

Davidson, L. A., B. G. Hoffstrom, et al. (2002). "Mesendoderm Extension and Mantle Closure in Xenopus laevis Gastrulation: Combined Roles for Integrin [alpha]5[beta]1, Fibronectin, and Tissue Geometry." Developmental Biology **242**(2): 109-129.

Davidson, L. A., R. Keller, et al. (2004). "Patterning and tissue movements in a novel explant preparation of the marginal zone of Xenopus laevis." Gene Expression Patterns **4**(4): 457-466.

De Marco, P., E. Merello, et al. (2006). "Current perspectives on the genetic causes of neural tube defects." neurogenetics **7**(4): 201-221.

Djiane, A., J. Riou, et al. (2000). "Role of frizzled 7 in the regulation of convergent extension movements during gastrulation in Xenopus laevis." Development **127**(14): 3091-3100.

Dzamba, B. J., K. R. Jakab, et al. (2009). "Cadherin adhesion, tissue tension, and noncanonical Wnt signaling regulate fibronectin matrix organization." Dev Cell **16**(3): 421-32.

Edwards, D. C. and G. N. Gill (1999). "Structural features of LIM kinase that control effects on the actin cytoskeleton." J Biol Chem **274**(16): 11352-61.

Effler, J. C., P. A. Iglesias, et al. (2007). "A mechanosensory system controls cell shape changes during mitosis." Cell Cycle **6**(1): 30-5.

Fanto, M. and H. McNeill (2004). "Planar polarity from flies to vertebrates." J Cell Sci **117**(4): 527-533.

Frydman, H. M. and A. C. Spradling (2001). "The receptor-like tyrosine phosphatase lar is required for epithelial planar polarity and for axis determination within drosophila ovarian follicles." Development **128**(16): 3209-20.

Geiger, B., J. P. Spatz, et al. (2009). "Environmental sensing through focal adhesions." Nat Rev Mol Cell Biol **10**(1): 21-33.

Gerisch, G., R. Albrecht, et al. (1995). "Chemoattractant-controlled accumulation of coronin at the leading edge of Dictyostelium cells monitored using a green fluorescent protein-coronin fusion protein." Curr Biol **5**(11): 1280-5.

Goto, T., L. Davidson, et al. (2005). "Planar Cell Polarity Genes Regulate Polarized Extracellular Matrix Deposition during Frog Gastrulation." Current Biology **15**(8): 787-793.

Green, J. B., I. Dominguez, et al. (2004). "Self-organization of vertebrate mesoderm based on simple boundary conditions." Dev Dyn **231**(3): 576-81.

Habas, R., I. B. Dawid, et al. (2003). "Coactivation of Rac and Rho by Wnt/Frizzled signaling is required for vertebrate gastrulation." Genes Dev **17**(2): 295-309.

Habas, R., Y. Kato, et al. (2001). "Wnt/Frizzled activation of Rho regulates vertebrate gastrulation and requires a novel Formin homology protein Daam1." Cell **107**(7): 843-54.

Hall, A. (2005). "Rho GTPases and the control of cell behaviour." Biochem. Soc. Trans. **33**(Pt 5): 891-895.

Hyodo-Miura, J., T. S. Yamamoto, et al. (2006). "XGAP, an ArfGAP, Is Required for Polarized Localization of PAR Proteins and Cell Polarity in Xenopus Gastrulation." Developmental Cell **11**(1): 69-79.

Ilan Spector, N. R. S. D. B. Y. K. (1989). "Latrunculins - novel marine macrolides that disrupt microfilament organization and affect cell growth: I. Comparison with cytochalasin D." Cell Motility and the Cytoskeleton **13**(3): 127-144.

Kandow, C. E., P. C. Georges, et al. (2007). Polyacrylamide Hydrogels for Cell Mechanics: Steps Toward Optimization and Alternative Uses. Methods in Cell Biology, Academic Press. **Volume 83:** 29-46.

Kaverina, I., O. Krylyshkina, et al. (1999). "Microtubule Targeting of Substrate Contacts Promotes Their Relaxation and Dissociation." J. Cell Biol. **146**(5): 1033-1044.

Kay, B. K. and H. B. Peng (1991). *Xenopus laevis*: practical uses in cell and molecular biology. New York, Academic Press.

Keller, R., L. Davidson, et al. (2000). "Mechanisms of convergence and extension by cell intercalation." Philosophical Transactions of the Royal Society of London Series B-Biological Sciences **355**(1399): 897-922.

Khadka, D. K., W. Liu, et al. "Non-redundant roles for Profilin2 and Profilin1 during vertebrate gastrulation." Developmental Biology **In Press, Accepted Manuscript**.

Kreis, T. E., B. Geiger, et al. (1982). "Mobility of microinjected rhodamine actin within living chicken gizzard cells determined by fluorescence photobleaching recovery." Cell **29**(3): 835-45.

Kwan, K. M. and M. W. Kirschner (2005). "A microtubule-binding Rho-GEF controls cell morphology during convergent extension of Xenopus laevis." Development **132**(20): 4599-610.

Laevsky, G. and D. A. Knecht (2003). "Cross-linking of actin filaments by myosin II is a major contributor to cortical integrity and cell motility in restrictive environments." J Cell Sci **116**(18): 3761-3770.

Lane, M. C. and R. Keller (1997). "Microtubule disruption reveals that Spemann's organizer is subdivided into two domains by the vegetal alignment zone." Development **124**(4): 895-906.

Lanzetti, L. (2007). "Actin in membrane trafficking." Curr Opin Cell Biol **19**(4): 453-8.

Lauffenburger, D. A. and A. F. Horwitz (1996). "Cell Migration: A Physically Integrated Molecular Process." Cell **84**(3): 359-369.

Leach, J. B., X. Q. Brown, et al. (2007). "Neurite outgrowth and branching of PC12 cells on very soft substrates sharply decreases below a threshold of substrate rigidity." Journal of Neural Engineering **4**(2): 26-34.

Litman, P., M. Amieva, et al. (2000). "Imaging of Dynamic Changes of the Actin Cytoskeleton in Microextensions of Live NIH3T3 Cells with a GFP Fusion of the F-Actin Binding Domain of Moesin." BMC Cell Biology **1**(1): 1 - 1.

Liu, J., M. Kaksonen, et al. (2006). "Endocytic vesicle scission by lipid phase boundary forces." Proc Natl Acad Sci U S A **103**(27): 10277-82.

Liu, W., A. Sato, et al. (2008). "Mechanism of activation of the Formin protein Daam1." Proceedings of the National Academy of Sciences **105**(1): 210-215.

Liu, Z., J. L. Tan, et al. (2010). "Mechanical tugging force regulates the size of cell-cell junctions." Proc Natl Acad Sci U S A **107**(22): 9944-9.

Martin, A. C., M. Kaschube, et al. (2009). "Pulsed contractions of an actin-myosin network drive apical constriction." Nature **457**(7228): 495-9.

Miyakoshi, A., N. Ueno, et al. (2004). "Rho guanine nucleotide exchange factor xNET1 implicated in gastrulation movements during Xenopus development." Differentiation **72**(1): 48-55.

Morgan, R., M. H. W. Hooiveld, et al. (1999). "A novel guanine exchange factor increases the competence of early ectoderm to respond to neural induction." Mechanisms of Development **88**(1): 67-72.

Mseka, T., J. R. Bamburg, et al. (2007). "ADF/cofilin family proteins control formation of oriented actin-filament bundles in the cell body to trigger fibroblast polarization." J Cell Sci **120**(Pt 24): 4332-44.

Nakaya, Y., E. W. Sukowati, et al. (2008). "RhoA and microtubule dynamics control cell-basement membrane interaction in EMT during gastrulation." Nat Cell Biol **10**(7): 765-75.

Nieuwkoop, P. D. and J. Faber (1967). Normal tables of *Xenopus laevis* (Daudin). Amsterdam, Elsevier North-Holland Biomedical Press.

Ninomiya, H., R. P. Elinson, et al. (2004). "Antero-posterior tissue polarity links mesoderm convergent extension to axial patterning." Nature **430**(6997): 364-7.

Ninomiya, H. and R. Winklbauer (2008). "Epithelial coating controls mesenchymal shape change through tissue-positioning effects and reduction of surface-minimizing tension." Nat Cell Biol **10**(1): 61-9.

Paluch, E., J. van der Gucht, et al. (2006). "Cracking up: symmetry breaking in cellular systems." J. Cell Biol. **175**(5): 687-692.

Pollard, T. D. (2007). "Regulation of Actin Filament Assembly by Arp2/3 Complex and Formins." Annual Review of Biophysics and Biomolecular Structure **36**(1): 451-477.

Pollard, T. D. and J. A. Cooper (1986). "Actin and actin-binding proteins. A critical evaluation of mechanisms and functions." Annu Rev Biochem **55**: 987-1035.

Puech, P. H., A. Taubenberger, et al. (2005). "Measuring cell adhesion forces of primary gastrulating cells from zebrafish using atomic force microscopy." J Cell Sci **118**(Pt 18): 4199-206.

Reichl, E. M., Y. Ren, et al. (2008). "Interactions between myosin and actin crosslinkers control cytokinesis contractility dynamics and mechanics." Curr Biol **18**(7): 471-80.

Rosenblatt, J., M. C. Raff, et al. (2001). "An epithelial cell destined for apoptosis signals its neighbors to extrude it by an actin- and myosin-dependent mechanism." Curr Biol **11**(23): 1847-57.

Rossman, K. L., C. J. Der, et al. (2005). "GEF means go: turning on RHO GTPases with guanine nucleotide-exchange factors." Nat Rev Mol Cell Biol **6**(2): 167-180.

Russ, J. C. (1999). The image processing handbook, CRC Press.

Sato, A., D. K. Khadka, et al. (2006). "Profilin is an effector for Daam1 in non-canonical Wnt signaling and is required for vertebrate gastrulation." Development **133**(21): 4219-4231.

Senju, Y. and H. Miyata (2009). "The Role of Actomyosin Contractility in the Formation and Dynamics of Actin Bundles During Fibroblast Spreading." J Biochem **145**(2): 137-150.

Shih, J. and R. Keller (1992a). "Cell motility driving mediolateral intercalation in explants of Xenopus laevis." Development **116**(4): 901-14.

Shih, J. and R. Keller (1992b). "Patterns of cell motility in the organizer and dorsal mesoderm of Xenopus laevis." Development **116**(4): 915-30.

Skoglund, P., A. Rolo, et al. (2008). "Convergence and extension at gastrulation require a myosin IIB-dependent cortical actin network." Development **135**(14): 2435-2444.

Slattum, G., K. M. McGee, et al. (2009). "P115 RhoGEF and microtubules decide the direction apoptotic cells extrude from an epithelium." J Cell Biol **186**(5): 693-702.

Small, J. V. and I. Kaverina (2003). "Microtubules meet substrate adhesions to arrange cell polarity." Current Opinion in Cell Biology **15**(1): 40-47.

Smutny, M., H. L. Cox, et al. (2010). "Myosin II isoforms identify distinct functional modules that support integrity of the epithelial zonula adherens." Nat Cell Biol **12**(7): 696-702.

Sokal, R. R. and F. J. Rohlf (1994). Biometry. New York, W.H.Freeman and Company.

Solnica-Krezel, L. and W. Driever (1994). "Microtubule arrays of the zebrafish yolk cell: organization and function during epiboly." Development **120**(9): 2443-55.

Sorzano, C. O. S., P. Thevenaz, et al. (2005). "Elastic registration of biological images using vector-spline regularization." Biomedical Engineering, IEEE Transactions on **52**(4): 652 - 663.

Tahinci, E. and K. Symes (2003). "Distinct functions of Rho and Rac are required for convergent extension during Xenopus gastrulation." Developmental Biology **259**(2): 318-335.

Tanegashima, K., H. Zhao, et al. (2008). "WGEF activates Rho in the Wnt-PCP pathway and controls convergent extension in Xenopus gastrulation." Embo J **27**(4): 606-617.

Trepat, X., M. R. Wasserman, et al. (2009). "Physical forces during collective cell migration." Nature Physics **5**(6): 426-430.

Viktorinova, I., T. Konig, et al. (2009). "The cadherin Fat2 is required for planar cell polarity in the Drosophila ovary." Development **136**(24): 4123-32.

Wallingford, J. B. (2006). "Planar cell polarity, ciliogenesis and neural tube defects." Hum. Mol. Genet. **15**(suppl_2): R227-234.

Wallingford, J. B., B. A. Rowning, et al. (2000). "Dishevelled controls cell polarity during Xenopus gastrulation." Nature **405**(6782): 81-85.

Wang, Y. L. (1987). "Mobility of filamentous actin in living cytoplasm." J Cell Biol **105**(6 Pt 1): 2811-6.

Witzel, S., V. Zimyanin, et al. (2006). "Wnt11 controls cell contact persistence by local accumulation of Frizzled 7 at the plasma membrane." J. Cell Biol. **175**(5): 791-802.

Wozniak, M. A. and C. S. Chen (2009). "Mechanotransduction in development: a growing role for contractility." Nature Reviews in Molecular Cell Biology **10**: 34-43.

Wulf, E., A. Deboben, et al. (1979). "Fluorescent phallotoxin, a tool for the visualization of cellular actin." Proc Natl Acad Sci U S A **76**(9): 4498-502.

Yam, P. T., C. A. Wilson, et al. (2007). "Actin myosin network reorganization breaks symmetry at the cell rear to spontaneously initiate polarized cell motility." J. Cell Biol. **178**(7): 1207-1221.

Zallen, J. A. (2007). "Planar Polarity and Tissue Morphogenesis." Cell **129**(6): 1051-1063.

Zallen, J. A. and E. Wieschaus (2004). "Patterned gene expression directs bipolar planar polarity in Drosophila." Dev Cell **6**(3): 343-55.

Zar, J. H. (1998). Biostatistical Analysis. Upper Saddle River, New Jersey, Prentice-Hall.

Zhou, J., H. Y. Kim, et al. (2009). "Actomyosin stiffens the vertebrate embryo during critical stages of elongation and neural tube closure." Development **136**: 677-688.

Zhou, J., H. Y. Kim, et al. (2010). "Macroscopic stiffening of embryonic tissues via microtubules, RhoGEF and the assembly of contractile bundles of actomyosin." Development **137**(16): 2785-2794.

Zhou, M. and Y.-L. Wang (2008). "Distinct Pathways for the Early Recruitment of Myosin II and Actin to the Cytokinetic Furrow." Mol. Biol. Cell **19**(1): 318-326.